GeoArabia, Vol. 13, No. 3, 2008
Gulf PetroLink, Bahrain

The Middle Miocene Fatha (Lower Fars) Formation, Iraq

Ali Ismail Al-Juboury and Tom McCann

ABSTRACT

The Middle Miocene Fatha Formation (previously Lower Fars Formation) in northern Iraq was deposited in a broad and shallow foreland basin adjacent to the Zagros and Taurus Mountains. It forms a transgressive-regressive sequence comprising numerous shallowing-upward cycles of alternating mudrocks, limestones, gypsum and/or anhydrite and halite. These cycles reflect rapid changes in accommodation space in settings that ranged from open and restricted hypersaline marine to continental (sabkha and fluvio-deltaic). In the marginal parts of the basin, continental siliciclastics (red and variegated marls, silts and fine sandstones) represent either aeolian deposition or a combined lagoonal- and/or fluvial-dominated delta system. Eustasy, rather than tectonics, caused the high-frequency cyclicity seen in the Fatha Formation. We present twelve sections dominated by evaporites from the Sinjar and Fatha sub-basins to represent the main lithologic constituents of the formation. Our detailed analysis of the sedimentary succession focuses on the three main lithofacies (siliciclastics, carbonates and evaporites). Petrographic, geochemical and scanning electron microscope analysis of these units are presented. We identified a range of carbonate lithotypes: marly, arenaceous (detrital), organic-rich (fossiliferous), dolomitic limestone and dolomite. Dolomitic limestones occur mostly in the lower part of the lower member of the formation, which was deposited in a barred lagoonal environment with high salinity. The presence of peloidal lime-wackestone with bioclasts, particularly in the upper part of the lower member of the formation, may reflect quiet, shallow-water marine conditions with moderate depths and low energy. The bioclastic-peloidal grainstone-packstone microfacies, with a common and diverse fossil assemblage, may reflect high to moderate energy, shallow-water environments. Evaporites comprise the main sediments of the Fatha Formation. Nodular gypsum is the dominant gypsum type, although laminated, thick-bedded, and secondary gypsum (selenite and satin spar) also occur. In the subsurface, anhydrite and halite are the principal minerals.

INTRODUCTION

The *Lower Fars Formation* was originally described in the Fars Province of Iran by Busk and Mayo (1918), but without a type locality (van Bellen et al., 1959). Accordingly, Jassim et al. (1984) proposed the name *Fatha Formation* to replace the *Lower Fars Formation* in Iraq and defined the type-section in the Al Fatha Gorge (10 km north of Baiji town, where the Tigris River crosses the Makhul-Hamrin Range, Figure 1). This recommendation was published by Al-Rawi et al. (1993) and was adopted by other authors (e.g. Jassim and Buday, 2006) and herein. The Middle Miocene Fatha Formation is one of the most regionally widespread formations in Iraq (Al-Juboury et al., 2001; Jassim and Buday, 2006). It is mainly evaporitic, consisting of numerous shallowing-upward cycles of alternating mudrocks, limestones, gypsum, anhydrite and halite (Figures 1 to 3). It forms an important component of the petroleum system because it provides a regional seal to numerous oil reservoirs in Iraq; in many fields it is a reservoir in its own right (e.g. Kirkuk field, Dunnington, 1958; Metwalli et al., 1974). In addition, the formation yields economically significant deposits of sulfur found in evaporite beds consisting mainly of gypsum and anhydrite, as well as sulfate and salt (Al-Sawaf, 1977; Barker et al., 1979; Jassim et al., 1999).

Because of its economic significance, the Fatha Formation has been described in numerous papers and several books (e.g. Dunnington, 1958; van Bellen et al., 1959; Shawkat and Tucker, 1978; Buday, 1980; Jassim and Buday, 2006), the majority of which focus on geological overviews of Iraq and/or describe certain lithofacies. We review several of these previous studies. We then examine in greater detail the petrography, geochemistry and diagenesis of the Fatha lithofacies in northern Iraq.

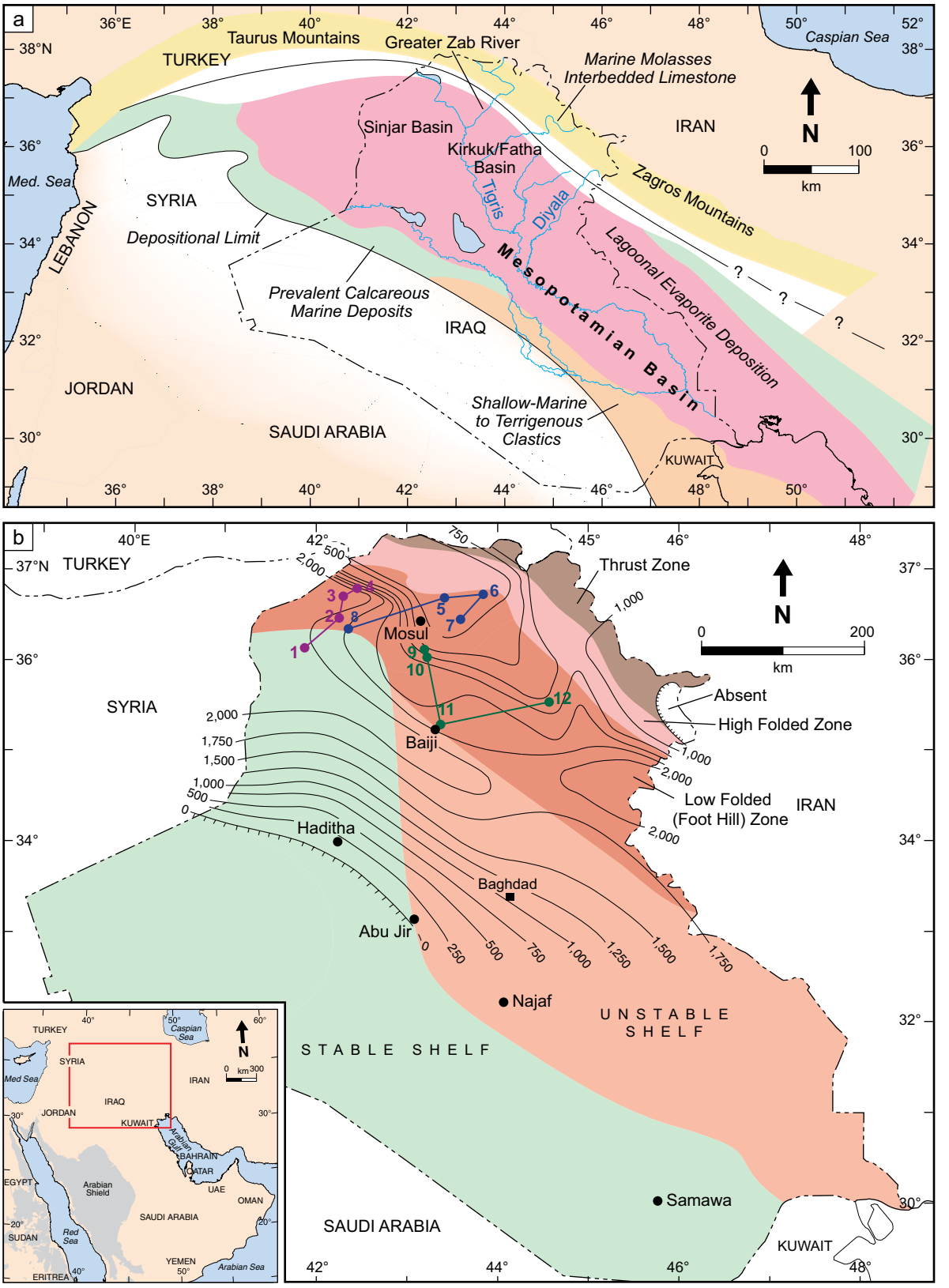

Figure 1: (a) Location map showing the Mesopotamian Basin in Iraq, and Fatha/Kirkuk and Sinjar sub-basins. Simplified Middle Miocene lithofacies distribution map (after Dunnington, 1958; Buday, 1973, 1980; Jassim and Karim, 1984; Hasan, 1985; Khalaf, 1988; Goff et al., 1995; Numan, 1997).

(b) Locations of the 12 studied sections: (1) Well 0-S; (2) Sasan; (3) Gusair; (4) Butma west; (5) Sheikhan; (6) Maqlub; (7) Bahzani; (8) Sheikh Ibrahim; (9) Hamam Al-Alil; (10) Mishraq Well 1; (11) Fatha type section; and (12) Well 00-S. Also shown is an isopach map of the Fatha Formation (after Dunnington, 1958) and tectonic provinces.

Twelve sections in northern Iraq were considered for the study (Figures 1 to 3), of which sections 8 (Sheikh Ibrahim) and 9 (Hamam Al-Alil, Figure 2) were found to best exhibit the various lithofacies and lithologies of the Fatha Formation. From these two sections, we collected 65 samples from various lithotypes for petrographic and geochemical analysis. Selected samples were analyzed by scanning electron microscopy (SEM) and X-ray diffraction (XRD, using D8 Advance [Bruker axs] with Cu-∞ radiation). Geochemical analysis of major and trace elements for selected samples was done using a Siemens SRS 303 X-ray fluorescence spectrophotometer.

LITHOSTRATIGRAPHIC DIVISIONS OF THE FATHA FORMATION

Different schemes have been used to divide the Fatha Formation into members and/or units (Figure 2). The first of these involved its division into several beds, from top to bottom (Daniel, 1954; Sugden, 1951; W. Kitchin, *in* van Bellen et al., 1959):

Upper Red Beds (up to 55 m thick) consist of eight limestone markers (designated R/8 to R/1) separated by siltstones and anhydrites. The top of the formation is marked by a prominant anhydrite that is informally designated as A0. A thick anhydrite bed occurs below the Upper Red Beds.

Seepage Beds (up to 40 m thick) consist of four limestone markers (designated B/4 to B/1) separated by siltstones and anhydrites.

Saliferous Beds (up to 25 m thick) consist of anhydrite/gypsum, halite, marl and limestone. Three basal limestone markers (designated S/3 to S/1) occur below the plastic halite unit.

Transition Beds (up to 185 m thick) consist of 14 limestone markers (designated T/13 to T/6, Z, T/5 to T/1)) separated by siltstones and anhydrites. Uppermost units T/1 to T/3 are locally absent due to either facies changes or pinchouts. In the Kirkuk structure, the lower markers are progressively cut out northwards, by onlap convergence.

Basal Fars Conglomerate, in northern Iraq, occurs at the base of formation, and is hereafter referred to as the *Basal Fatha Conglomerate*.

The upper four beds were recognized in the Kirkuk field, where the thickness of the formation is about 1,000 ft (305 m) in the northwest and 2,000 ft (610 m) in the southwest. Farther to the northeast (Figure 1a), the units lose their evaporitic character (van Bellen et al., 1959; Al-Rawi et al., 1993).

A second regional scheme, used by research teams working for the Directorate General of the Geological Survey and Mineral Investigation, involves two members (Figure 2, Taufiq and Domas, 1977; Al-Mubarak and Youkhana, 1977; Mohi Al-Din et al., 1977; Hagopian and Vejlupek, 1977). The lower member consists of rhythmic alternations of marl, limestones, and gypsum, while the upper member is similar, but with additional red siliciclastics, including sandstone, siltstone, and claystone.

According to Jassim and Buday (2006), in the Fatha type section, the Lower Member is 220 m thick and includes: (1) a 40-m-thick basal unit of organo-detrital limestone and anhydrite (or gypsum), green dolomitic marl and thin limestone; and (2) a 100-m-thick section of cyclically interbedded gypsum, green marl and limestone. These two units would appear to correspond to the Transition and Seepage Beds with the intervening Saliferous Beds absent by non-deposition, lateral facies change or dissolution. In the type section, the Upper Member is 400 m thick and consists of cyclic red and green mudstones, gypsum and thin oolitic limestone beds, with calcarenite beds at the top. The present study adopts this two-member scheme for sections of the Sinjar Basin where the formation exceeds 600 m in thickness (Jassim and Buday, 2006).

A third scheme was used by Ma'ala et al. (1988) for detailed regional mapping. They recognized five laterally persistent limestone marker beds within the Fatha Formation. *Marker Beds 1 and 2* are located in the lower member while *Marker Beds 3, 4 and 5* are within the upper (Figure 2). All of the marker beds are characterized by particular lithological properties: Marker Bed M1 is a marly limestone, partly dolomitic; Marker Bed M2 consists of two limestone horizons with gypsum or marl in between;

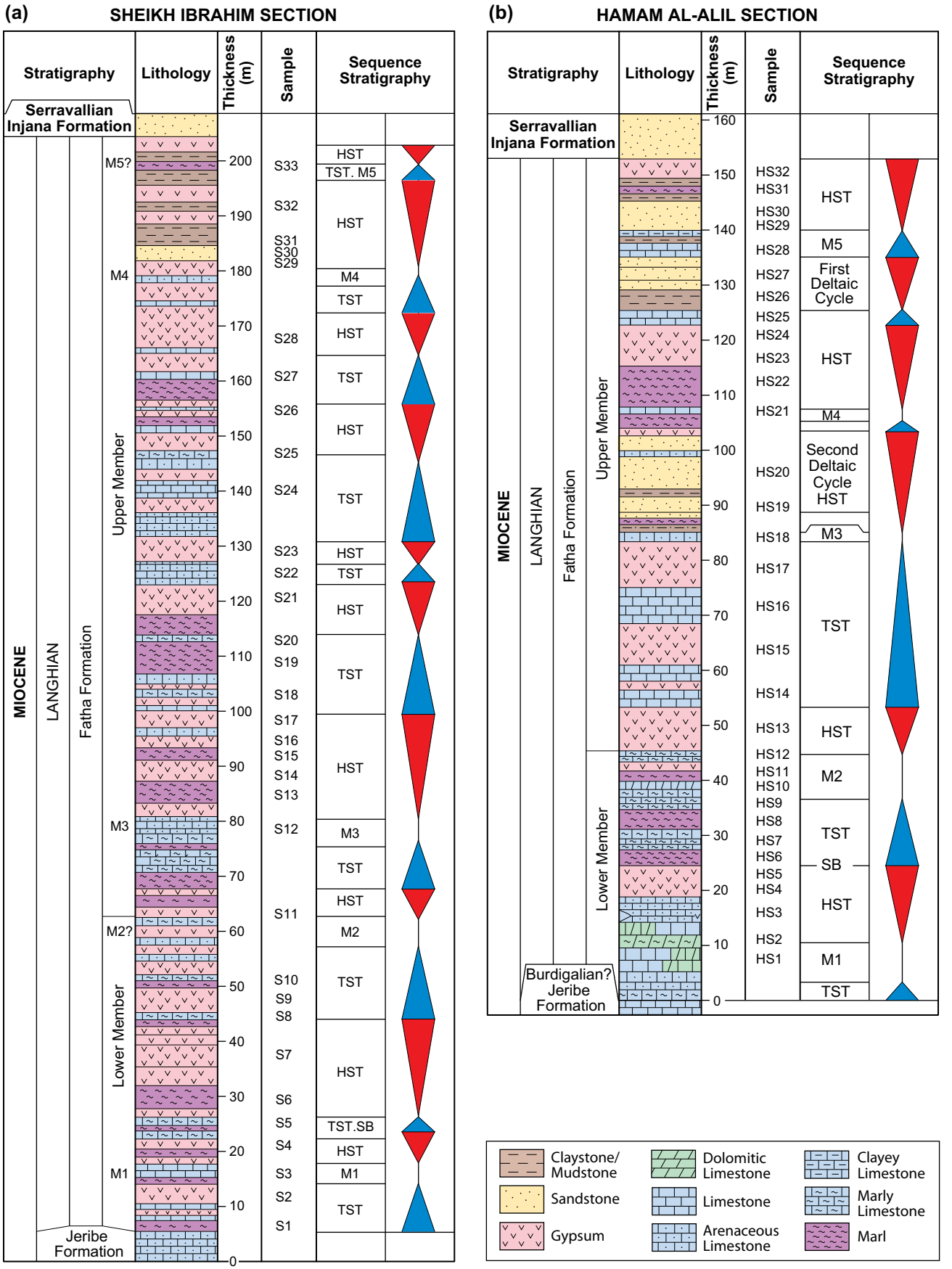

Figure 2: Composite lithologic section of the Fatha Formation in the Hamam Al-Alil and Sheikh Ibrahim sections (see Figures 1 and 3 for locations). The five Limestone Marker Beds M1 to M5 can generally be correlated in the study area (Ma'ala et al., 1988). Higher-order sequences are also shown, including the two deltaic sequences and sample locations.

Marker Bed M3 is a crystalline limestone; Marker Bed M4 is an arenaceous and marly limestone; and Marker Bed M5 is a fossiliferous marly limestone (Figure 2). This subdivision is used in the present work for sections 9-11, which lie between Fatha and Mosul (i.e. in the Fatha Basin, a sub-basin of the Kirkuk Basin, and for sections 2, 3, 4 and 8 of Sinjar Basin).

Lower Boundary and Underlying Formation

Where the Miocene stratigraphic succession is complete, the Fatha Formation conformably overlies the Lower Miocene (Burdigalian?) Jeribe Formation (Figures 2 and 3). In some localities in northern Iraq (e.g. section 5, Sheikhan in Figure 3c), the lower part of the Fatha Formation consists of the *Basal Fars Conglomerate* (van Bellen et al., 1959; here renamed the *Basal Fatha Conglomerate*). The conglomerate occurs above a "middle Eocene-lower Miocene" unconformity (van Bellen et al., 1959). As seen in several localities in Figure 3, the unconformity is evident where the Fatha Formation overlies the Eocene Pila Spi or Lower Miocene Euphrates formations (i.e. Jeribe Formation is absent). Thinning of the Fatha Formation (sections 5 and 6, Figure 3c) is due to onlap onto a paleohigh. The Basal Fatha Conglomerate also thins out and virtually disappears in a basinward direction (van Bellen et al., 1959). These conglomerates are occasionally associated with paleosols, formed mainly of dolocrete (Al-Delemi, 2006).

Upper Boundary and Overlying Formation

The Upper Miocene Injana Formation (formerly Middle and Upper Fars formations) overlies the Fatha Formation. The Injana Formation is essentially a clastic sequence, consisting of fining-upwards cyclothems of sandstone, siltstone, marl and claystone (Al-Juboury, 1994). The lowermost part of Injana Formation consists of approximately 20 m of transitional fluvio-deltaic facies with significant channel development. This coarser interval may be related to the encroachment of clastic sediments into the Fatha Formation lagoonal setting.

LITHOFACIES AND DEPOSITIONAL SETTINGS

We examined the Fatha Formation in terms of three main lithofacies (following the system of Al-Naqib and Aghwan, 1993). These are:

(1) Clastics: Mudrocks (Marls) and Red Siliciclastics;
(2) Carbonates: Marly Limestone, Arenaceous Limestone and Limestone/Dolomite;
(3) Sulphates: Nodular Gypsum, Laminated Gypsum and Secondary Gypsum.

Clastics: Mudrocks

The mudrocks are carbonate-rich, and include marls, silty marls and sandy marls. These occur in beds 0.1–4.5 m thick in the lower member to 7.0 m in the upper member. The sediments are laminated to thickly bedded and commonly exhibit conchoidal fracture. They contain abundant fossils, including gastropods, pelecypods and oysters. Fossil populations and sizes decrease gradually upwards, accompanied by an increase in the frequency and size of gypsum nodules within the marl.

The mudrocks are grey, green or yellow; the yellowish grey marl is sometimes referred to as the *Basal Marl* because it is generally found at the base of high-frequency cycles. The contact between this basal marl and the overlying gypsum beds is usually irregular and erosional, while the contact with limestone beds is gradational, reflecting a flooding event.

Petrographically, the silty marl is composed of silt-sized quartz and feldspar grains in a groundmass of clayey and carbonate material. In thin section, the color is frequently red (Figure 4a). Scanning electron images show that the quartz is embedded within the carbonate cement (Figure 4b); authigenic dolomite rhombs are also observed (Figure 4c). The clay mineral assemblage is dominated by illite, kaolinite and authigenic palygorskite (Figure 4d to 4f). Mineralogically, the marls are composed of calcite, dolomite, quartz, feldspar and clay minerals, as shown by XRD analysis (Figures 5a and 5b). Clay minerals include palygorskite, illite, kaolinite and chlorite (Al-Juboury et al., 2001).

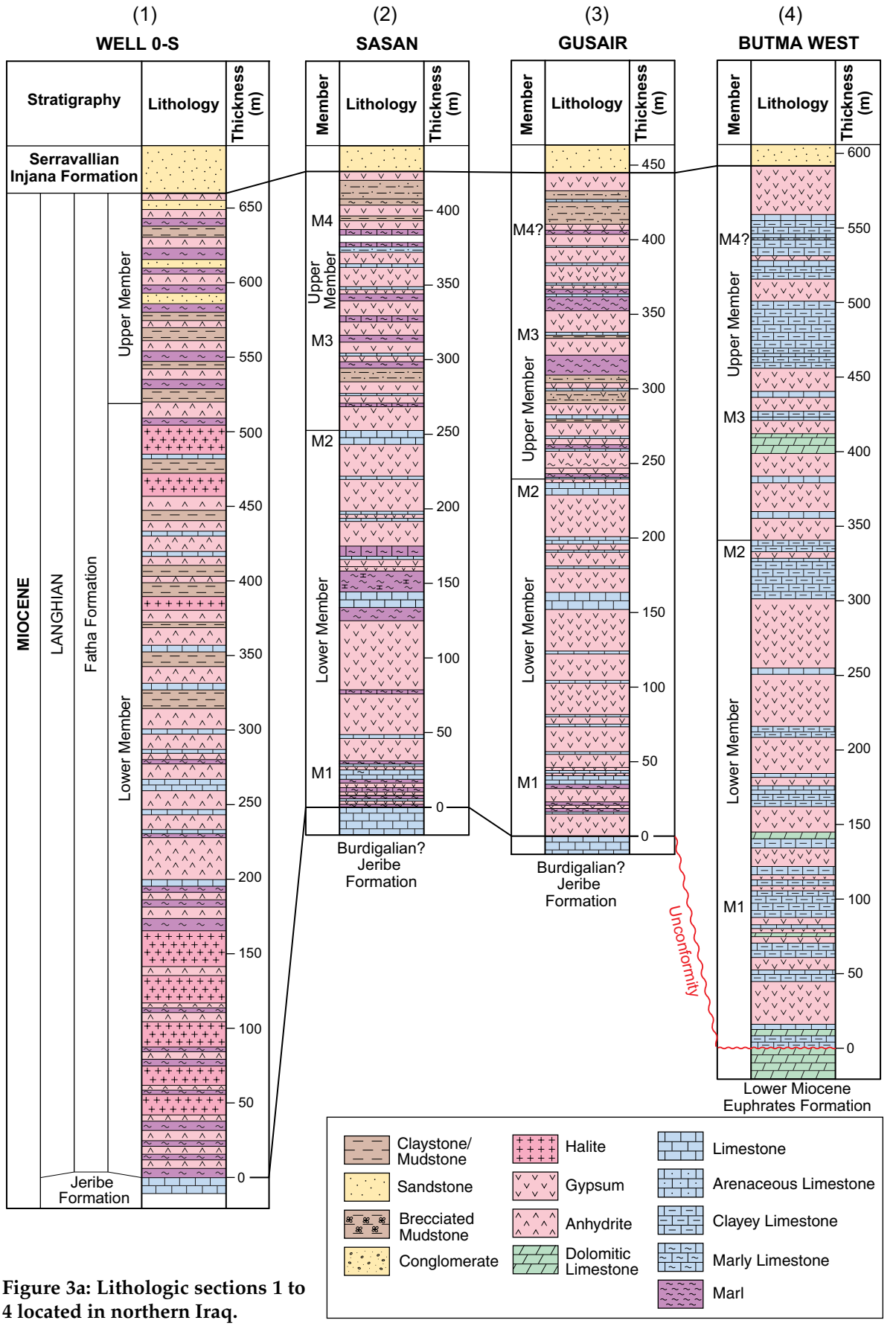

Figure 3a: Lithologic sections 1 to 4 located in northern Iraq.

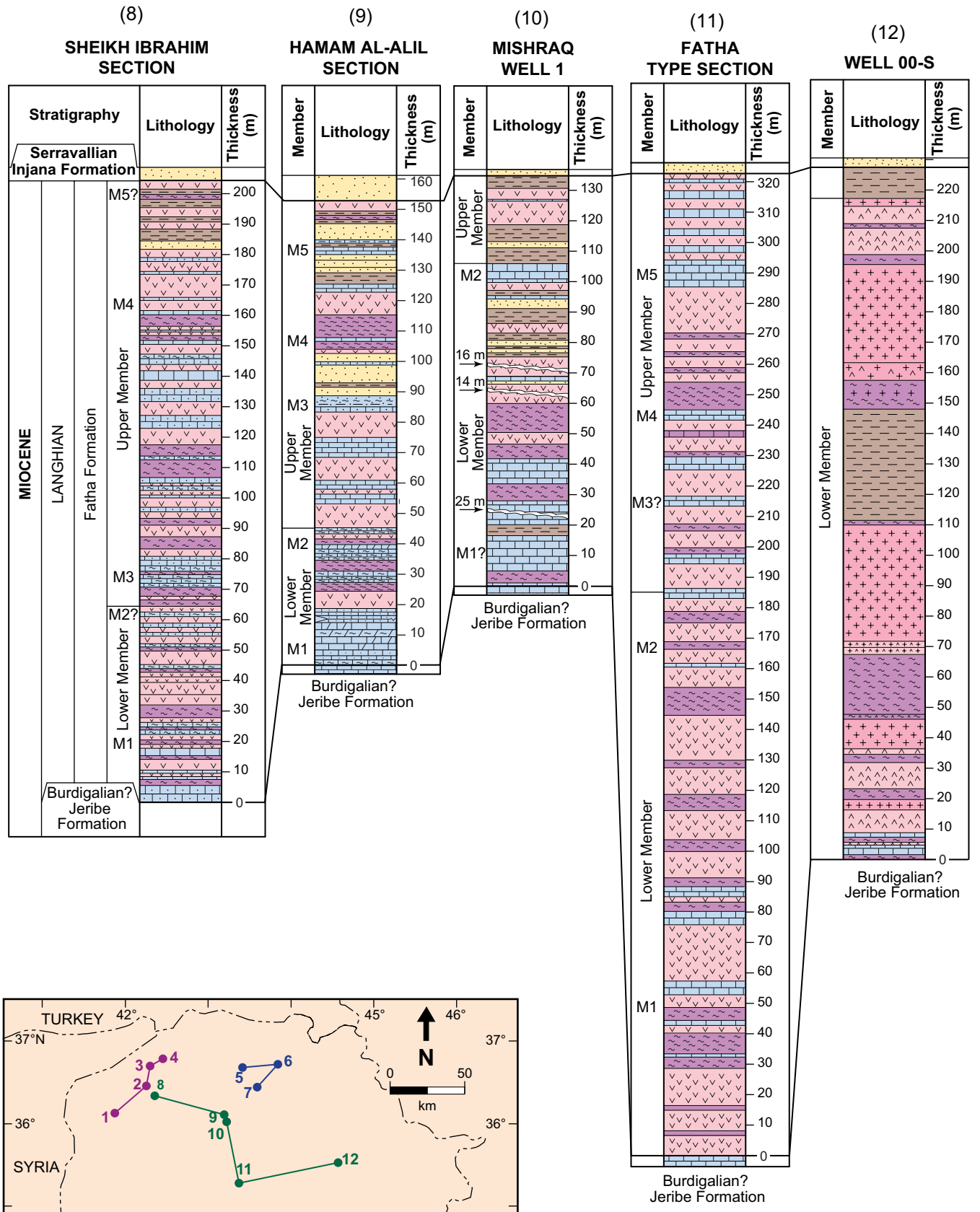

Figure 3b: Lithologic sections 8 to 12 located in northern Iraq.

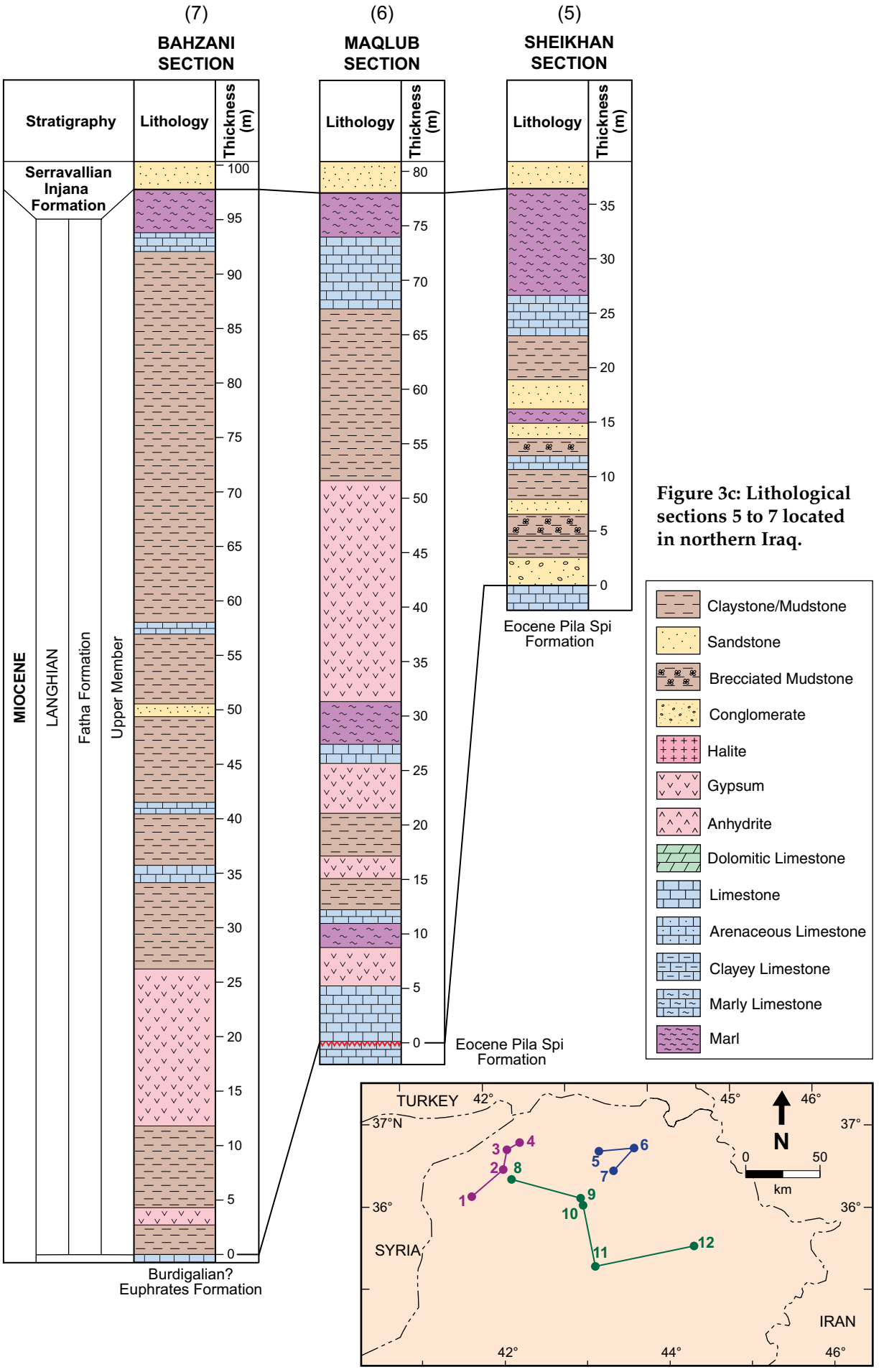

Figure 3c: Lithological sections 5 to 7 located in northern Iraq.

Table 1 shows the geochemical (XRF) analyses of selected marl samples. The chemical composition indicates that the yellow marls have higher CaO and lower SiO_2 content than the green. These results are confirmed by XRD analysis (i.e. high calcite and quartz content, Figure 5). The greenish marl also contains higher barium and strontium ratios compared to the yellow marls. Most major and trace elements are concentrated in the insoluble residues of these marls, mostly within the clay minerals.

Continuous reaction of sulphuric acid (formed by H_2S oxidation above the water table) with the clay minerals and carbonates in the Fatha marl resulted in acidification products alunite and jarosite with silica (ninivite), which constitutes an important indicator of alteration under low temperature-pressure conditions. The alteration pattern displays a zonation with a siliceous central part (ninivite) rimmed by alunite and fringed by jarosite and iron oxides (Jassim and Al-Naqib, 1989; Aswad et al., 1995). Association of the alteration products and their occurrence in the exclusively sedimentary sequence of marl, limestone and gypsum may indicate the occurrence of sulphur and predict H_2S seepage associated with hydrocarbons (Al-Juboury et al., 2006).

Depositional Setting: subtidal, reflecting restricted to open-marine environments. Ma'ala et al. (1988) interpreted the oysters as fauna that inhabited a brackish-water lagoon. The grey to yellowish marls indicate open-marine conditions.

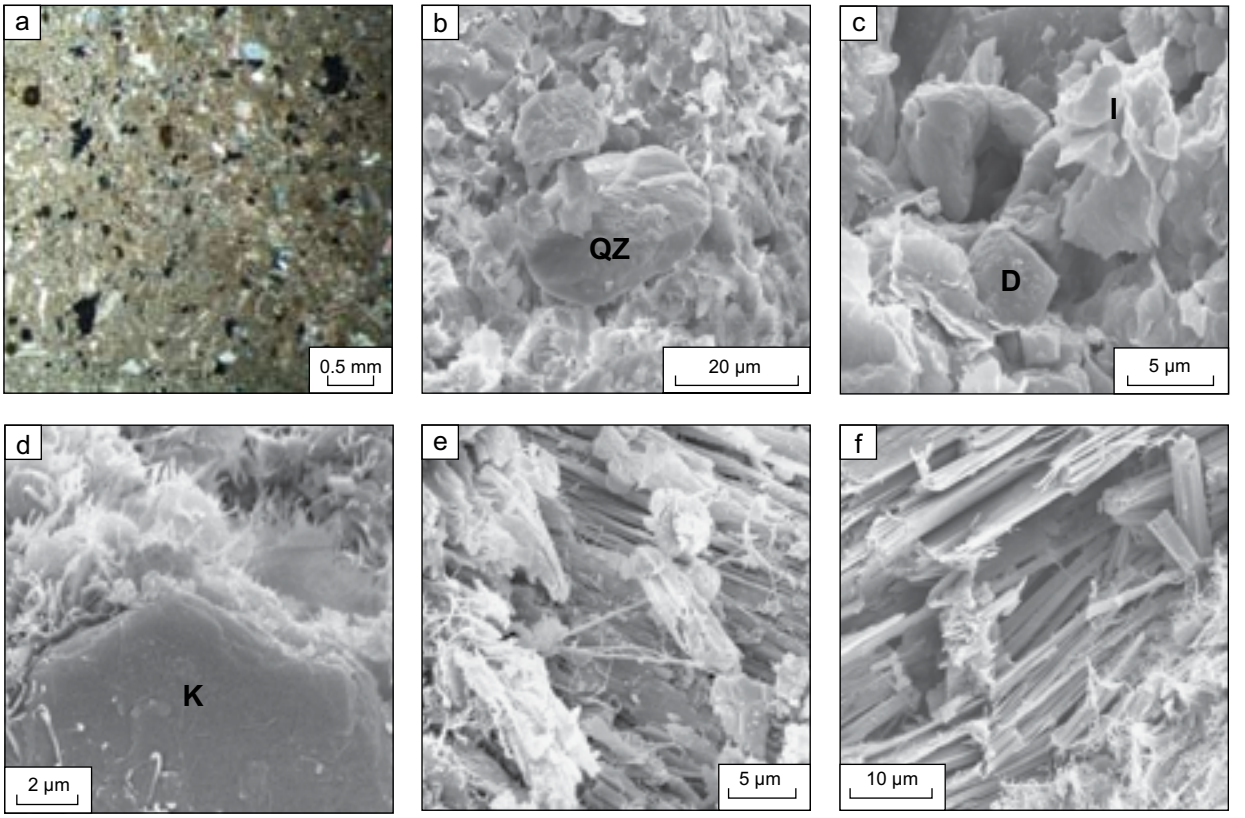

Figure 4: Photomicrographs showing:
(a) silt-sized quartz and feldspar floating in a groundmass of clayey and carbonate materials, generally of red colour. Hamam Al-Alil section, silty clay bed (M5, sample HS28).
(b) SEM image of quartz (QZ) embedded in carbonates with clayey fibreous minerals, yellow marl of Hamam Al-Alil section (sample HS22).
(c) SEM image shows dolomite rhomb (D) and clayey material (illite flakes, I) with carbonates in the yellow marl.
(d) SEM image shows kaolinite hexagonal form (K) and authigenic palygorskite fibers, silty marl of M5 at Hamam Al-Alil section.
(e) SEM image of long palygorskite fibers and carbonate fragments in the silty marl of M5.
(f) SEM image of the fibrous nature of the clayey materials, generally broken, in the silty marl of M5 with the presence of palygorskite/sepiolite in framboidal shapes.

Table 1: Distribution of major oxides and some trace elements in Fatha Marls.

Oxides %	Green Marl		Yellow Marl	
	Sheikh Ibrahim Section 8	**Hamam Al-Alil** Section 9	**Sheikh Ibrahim** Section 8	**Hamam Al-Alil** Section 9
SiO_2	52.07	40.31	25.83	35.21
TiO_2	0.84	0.63	0.43	0.60
Al_2O_3	12.31	9.67	6.37	9.95
Fe_2O_3	6.39	7.22	3.21	6.80
CaO	1.26	13.15	17.85	22.63
MgO	7.56	8.47	12.66	3.12
Na_2O	0.49	0.55	0.23	0.30
K_2O	3.28	2.11	1.72	2.54
MnO	0.03	0.10	0.03	0.07
P2O5	0.14	0.10	0.11	0.09
Trace elements ppm	**S15**	**HS31**	**S6**	**HS22**
Ba	348	282	115	204
Sr	1700	234	131	110
Rb	91	61	43	78
Ni	192	340	42	88
Cr	202	322	64	148
Co	17	26	04	13
Cu	60	75	45	72
V	507	569	479	636

Clastics: Red Siliciclastics

Red siliciclastics (sandstones and claystones) occur in the upper member of the Fatha Formation. The sandstones are quartz-rich (both mono- and poly-crystalline) (31.5%), with subsidiary feldspar, both plagioclase and orthoclase (9.8%). Lithic fragments (13.0%) include fragments of carbonates (4.5%), metamorphics (4.0%), chert (3.1%) and igneous rocks (1.4%). A clay-rich matrix and cement (mainly of calcite, but also ferruginous, clayey and gypsiferous) comprises about 43.5% of the total components. Accessory fractions (maximum 2.0%) include bioclastic fragments, glauconite, mica and heavy minerals. The heavy minerals include opaques (magnetite, chromite, ilmenite and hematite) and non-opaques (epidote, amphibole, pyroxene, garnet, staurolite, kyanite, muscovite, biotite, chlorite, zircon, tourmaline and rutile) (Al-Juboury et al., 2001). Figures 6 and 7 show the SEM images for the main constituents of the sandstones.

The sandstones contain a significant proportion of carbonate, both as cement and as rock fragments (Figure 8). Sometimes, the sandstone contains gypsum in the form of aggregates, either fine-grained micro-lenticular gypsum (gypsilutite) or coarse-grained micro-lenticular (gypsarenite, Figure 8e). These aggregates form micro-lenticular textures of optically homogeneous monocrystals with small calcite crystals growing on the boundaries (Figures 8d and 8e) and of non-oriented structures similar to those described by Salvany et al. (1994) for non-marine evaporites of the Ebro Basin, Spain.

The claystones are composed of quartz, calcite, feldspar and clay minerals. Detailed clay mineral analysis showed that the main clay mineral assemblage includes palygorskite, illite, kaolinite, and chlorite (Al-Juboury et al., 2001). Figure 9 shows SEM images for the common clay minerals, with quartz and feldspar embedded in the clay and carbonate groundmass.

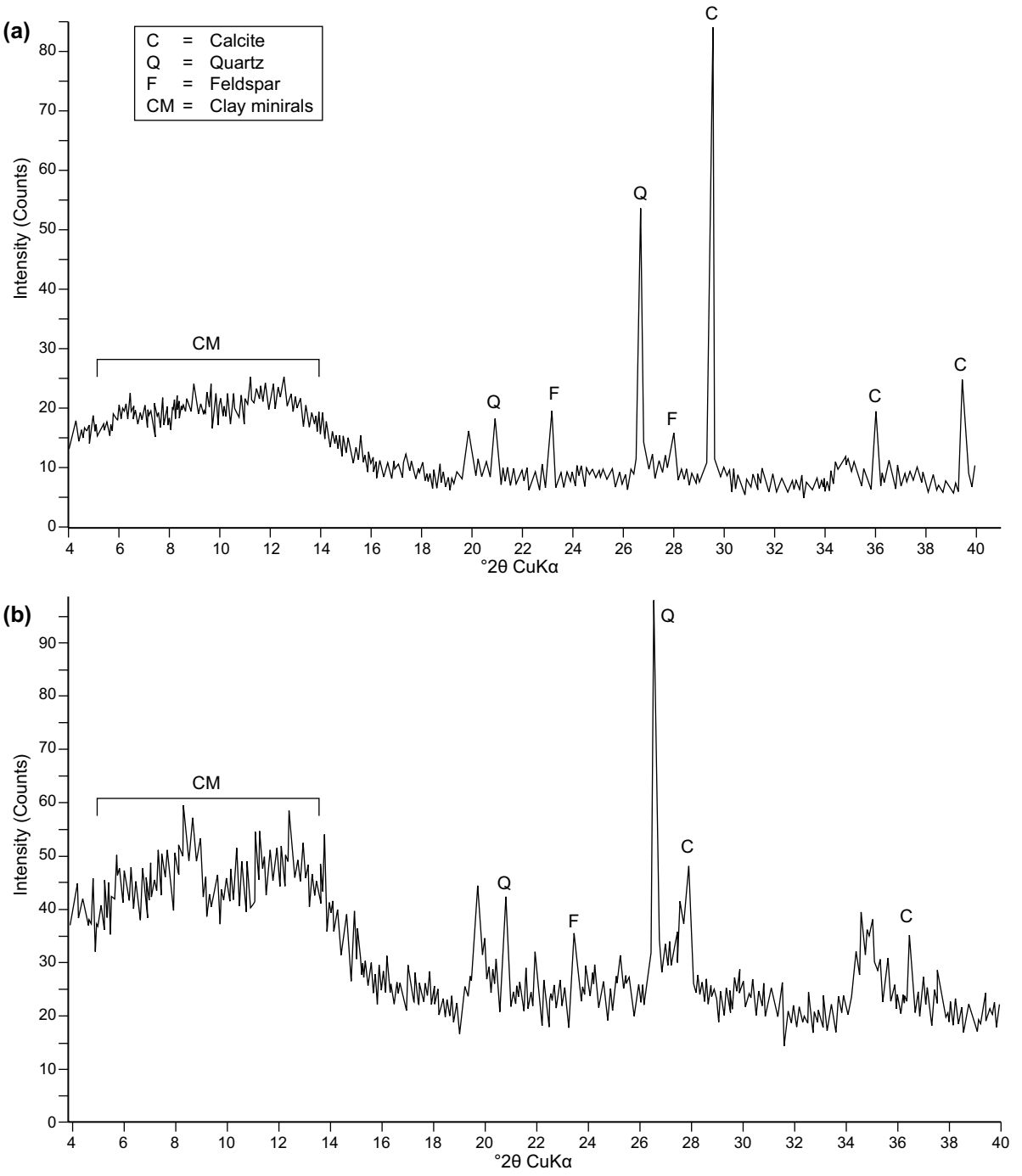

Figure 5: X-ray diffractograms of bulk samples from the Hamam Al-Alil section (see Figure 2): (a) yellow marl (sample HS22) and (b) green marl (sample HS6).

The geochemical compositions of selected sandstone samples are outlined in Table 2. The clastics are carbonate-rich, as indicated by the high content of CaO and MgO. Carbonate is present as calcite and dolomite cement as well as carbonate rock fragments (Figure 8). In general, the red clastics contain higher amounts of TiO_2, Al_2O_3 and Fe_2O_3. The TiO_2/Al_2O_3 ratio is relatively reduced in the red clastics compared with the grey and green clastics.

Depositional Setting

The quartz-rich sandstones represent fluvio-deltaic deposits, probably with a provenance from uplifted regions in the Zagros and Taurides Mountain belts (Jassim and Karim, 1984; Aqrawi, 1993). The red siliciclastics form the dominant lithology in the marginal part of the Mesopotamian Basin.

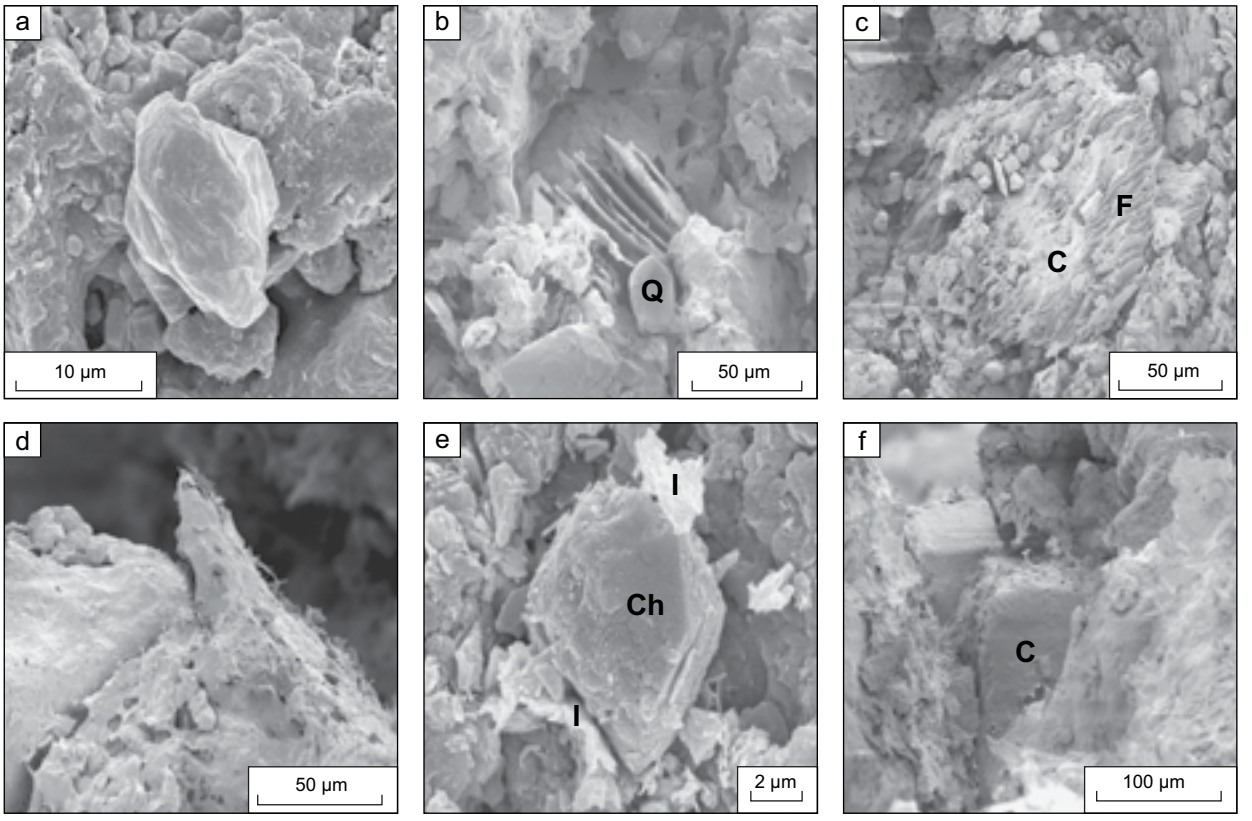

Figure 6: Scanning electron photoimages of the main constituents of the studied sandstones.
(a) Quartz grain with secondary overgrowth in carbonate cement (Hamam Al-Alil section, sample HS27).
(b) Relicts of feldspar after dissolution (centered) and hexagonal quartz (Q); note clay minerals on the surface of dissolved feldspar grain. All grains are embedded in carbonate cement (Sheikh Ibrahim section, sample S29).
(c) Corrosion of feldspar grain (F) and replacement by carbonate (C) in Sheikh Ibrahim section (sample S31).
(d) Clayey (illite) materials cementing detrital grains in sandstone; note the presence of small fibers of palygorskite.
(e) Chert fragment (Ch) embedded with illite flakes (I) in carbonate cement. Fine-grained gray sandstone.
(f) Carbonate crystals (calcite, C) filling vein in coarse-grained sandstone (images d-f from Hamam Al-Alil section, sample HS 29).

These occur at the tops of high-frequency cycles, are structureless and contain few organic remains. They may represent aeolian deposits and/or mixed lagoonal/fluvial and delta deposits. The red clastics were oxidized in an arid, episodically emergent, continental environment. These conditions were responsible for the overall increase of many of the major and trace elements in the red clastics. This is because the iron oxides and hydroxides adsorbed high concentrations of trace elements in their lattices (Krauskopf, 1979).

The upper member comprises sandstone, silty claystone and claystones and contains two coarsening-upward cycles (Al-Naqib and Aghwan, 1993). The older coarsening-upward ***Second Deltaic Cycle*** formed during a period of delta progradation within the lagoonal sediments. It occurs below the M4 Limestone Marker and ranges in thickness from 7.5–12.5 m; from base-up it consists of (Figure 2):

Unit 1: 3.0 m thick, finely-laminated, yellowish brown claystone and silty claystones;
Unit 2: 2.0 m thick, very fine, grey to brown, internally cross-bedded sandstone, gradually coarsening upwards into,

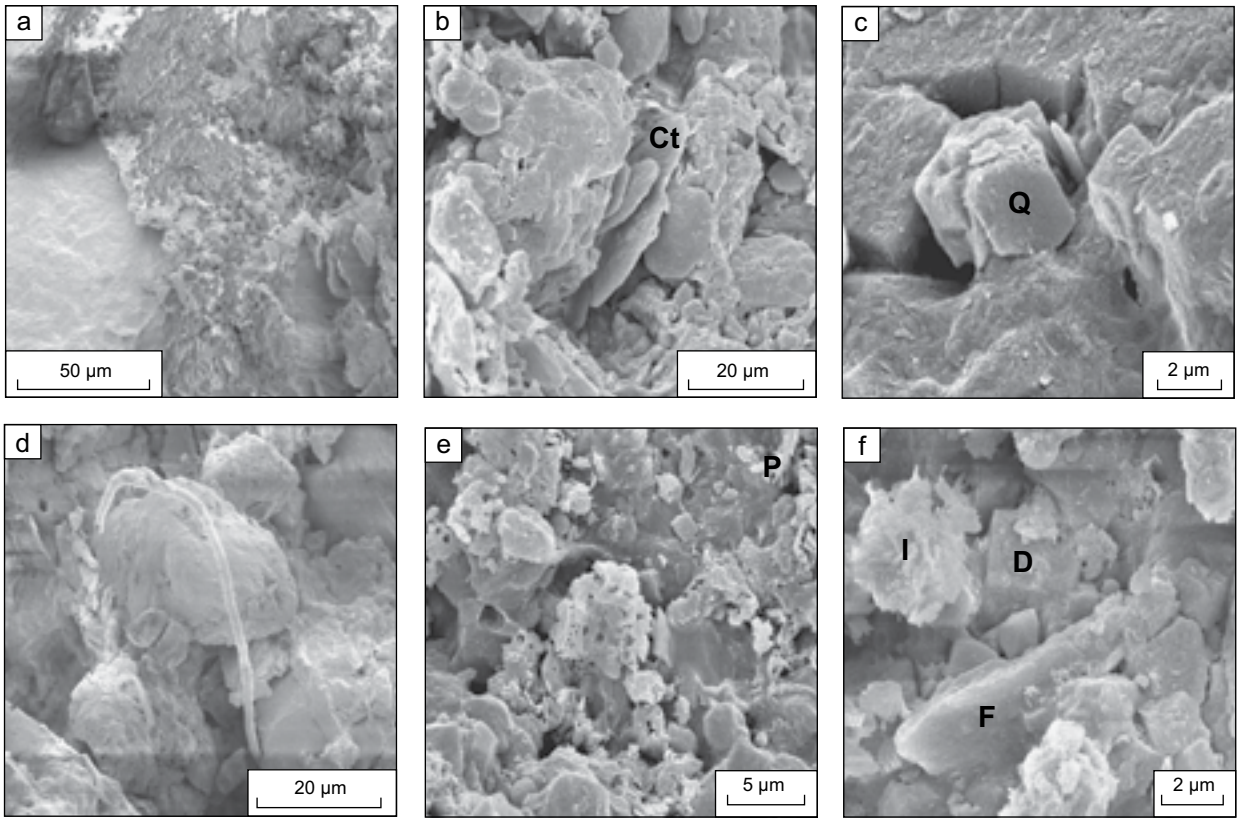

Figure 7: Scanning electron photoimages of the studied sandstones.
(a) Iron oxide pigment on quartz grain. Coarse-grained grey sandstone in Hamam Al-Alil section (sample HS 27).
(b) Disc-shaped chlorite mineral (Ct) in cavities between framework grains in grey friable sandstone in Sheikh Ibrahim section (sample S29).
(c) Quartz (Q) surrounded by calcite cement with short palygorskite fibers on the grain surfaces, porous fine-grained sandstone in Hamam Al Alil section.
(d) Palygorskite filling cavities in sandstone, and very well rounded carbonate rock fragment (C). Fine sandstone from Hamam Al-Alil section.
(e) Fossil remains in the center of photo with carbonate cement and palygorskite bundle of fibers (P) at right top, fine sandstone as in (c) and (d) above.
(f) Long feldspar grain (F), illite flakes (I) and dolomite rhomb (D) in calcite-rich fine sandstone (images c to f from Hamam Al-Alil section, sample HS 27).

Unit 3: 3.0 m thick, medium-grained sandstone, rippled, micro-cross-laminated and bioturbated (*Skolithos*) sediments;
Unit 4: 1.25 m of coarse-grained, thinly laminated sandstone;
M4 Marker: 2.8 m thick, with an upper yellowish brown, porous, fossiliferous limestone, and a lower bedded marly limestone.

The basal Unit 1 claystones represent a prodelta facies, while the silty claystones (Unit 1) and fine sandstones (Unit 2) represent delta-front facies. Changes in both grain size and lithology may be related to progradation of a distributary-channel mouth (Al-Juboury et al., 2001). The overlying cross-bedded sandstones (Unit 3) contain abundant *Skolithos* burrows that have been interpreted as shallow-marine, brackish-water deposits (Seilacher, 1967; Curran, 1985). A study of the various ichnofacies from the Fatha and overlying Injana formations revealed the occurrence of three distinct zones: the lower *Planolites* ichnofacies and upper *Skolithos* ichnofacies of the Fatha Formation, and the *Scoyenia* ichnofacies of the Injana Formation. These have been interpreted in terms of a broad shallowing-upward sequence from a semi-restricted lagoonal (*Planolites* ichnofacies) to brackish (*Skolithos* ichnofacies) to non-marine fluvial (*Scoyenia* ichnofacies) setting (Lawa, 1995).

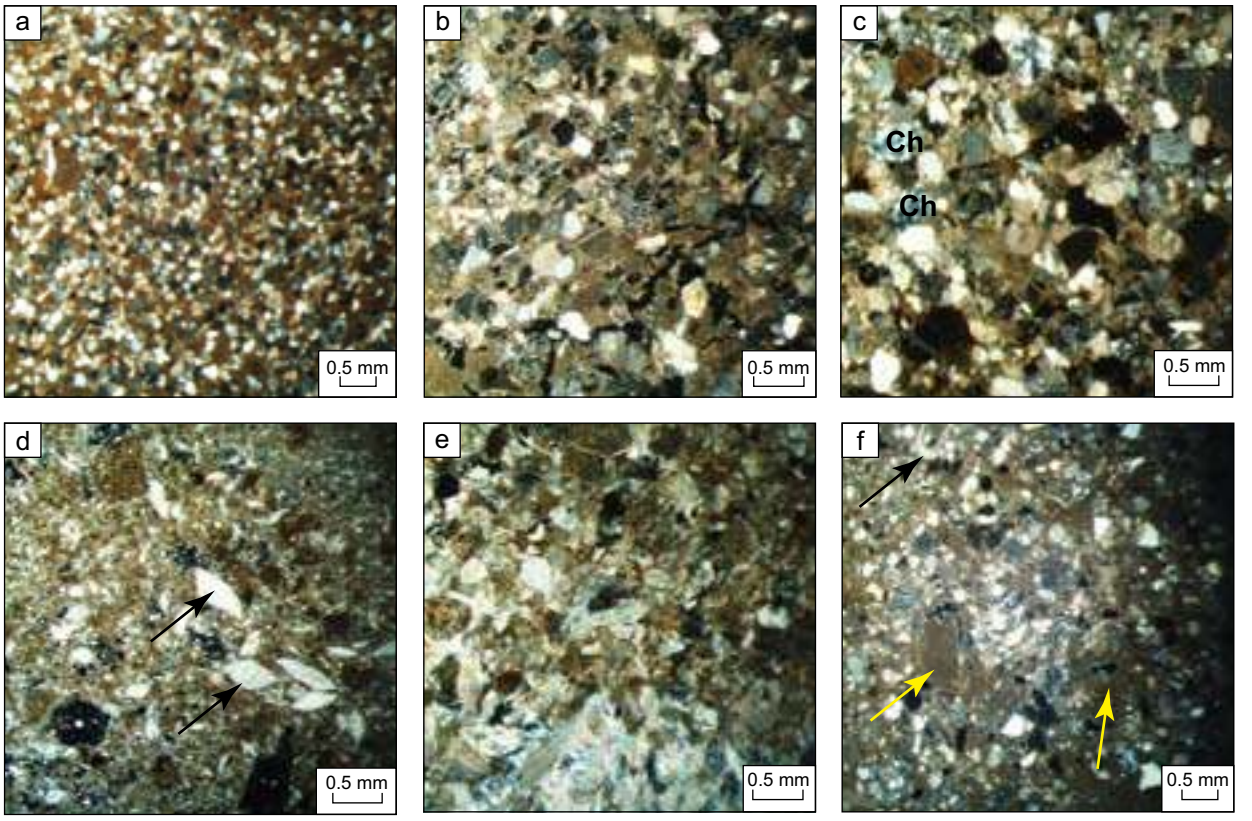

Figure 8: Photomicrographs of common constituents of Fatha carbonate–rich sandstones.
(a) Fine-grained sandstone (brown to grey) includes: quartz, both mono and polycrystalline with chert rock fragments and few feldspar in carbonate (calcite) cement.
(b) Medium-sized sandstone with the same components as above.
(c) Coarse-grained sandstone with more chert rock fragments (Ch) and igneous rock framents in carbonate cement. Photos (a to c) taken from deltaic cycle sandstone below M4 at Hamam Al-Alil section (sample HS20, Figure 2).
(d) Gypsilutite (fine microlenticular gypsum, arrows) in fine sandstone (green) forming the start of deltaic cycle at Sheikh Ibrahim section.
(e) Gypsarenite (coarse microlenticular gypsum) and fibreous gypsum in medium size sandstone in Sheikh Ibrahim section (sample S30).
(f) Remains of fossil (black arrow) and micritic carbonate rock fragments (yellow arrows) in fine sandstone (yellowish brown). Quartz grain is subangular with common chert rock fragments in carbonate cement, Hamam Al-Alil section (sample HS29).

The uppermost sandstone (Unit 4) may represent upper delta plain deposits that formed following a reduction in current velocity as flowing water entered a stagnant water body (e.g. lagoon). A marine flooding event temporarily reduced clastic input into the basin and deposited the M4 Limestone Marker in a low-energy marine (restricted) environment. According to Al-Naqib and Aghwan (1993), the mean palaeocurrent direction was towards 242°.

The younger *First Deltaic Cycle* comprises a broadly coarsening-upward siliciclastic sequence capped by the M5 Marker Bed. It ranges in thickness from 7.0–13.2 m; in Hamam Al-Alil it is 8.5 m thick; from base up, it consists of (Figure 2):

Unit 1: 1.0 m thick, red claystone grading to;
Unit 2: 50 cm thick, cross-laminated siltstone and fine-grained ripple-laminated sandstones grading to;
Unit 3: 6.0 m thick, fine-grained, yellowish brown cross-bedded sandstone;
Unit 4: 1.0 m thick, claystone.

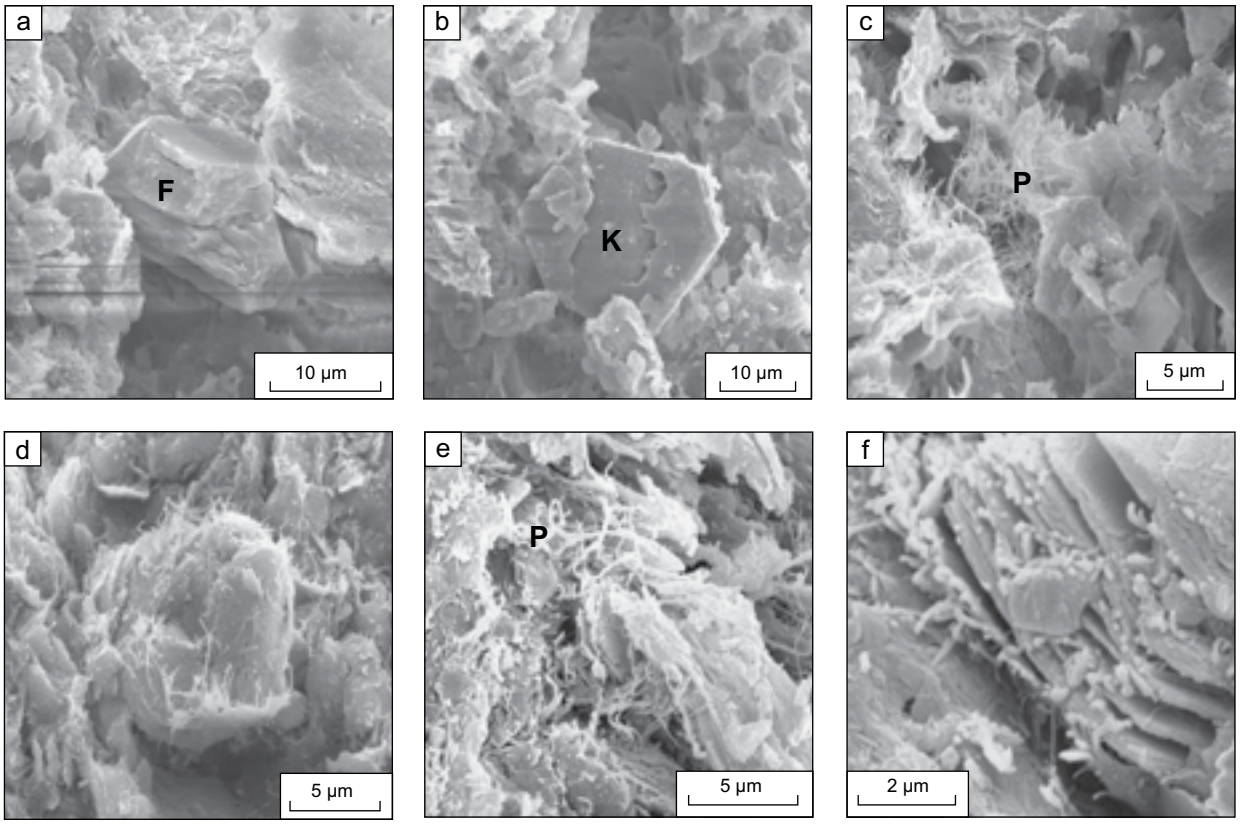

Figure 9: SEM images of claystones.
(a) Feldspar grain (F) in clayey and carbonate groundmass. Red claystone at Sheikh Ibrahim section (sample S29).
(b) Hexagonal plates of kaolinite (K) with corroded surfaces in red claystone, same sample as above.
(c) Palygorskite/sepiolite with tree-like texture (P) filling cavities in red claystone, same sample as above.
(d) Flakey and fibreous illite in framboidal shape (centered).
(e) Long and flexuous bundles of palygorskite fibers (P) indicating authigenic formation.
(f) Palygorskite fibers stacked with well-developed hexagonal kaolinite plates (images d-f from grey claystone in Hamam Al-Alil section, sample HS26).

M5 Marker, (1.0-3.0 m thick), divided into a limestone and an underlying silty marl. The limestone bed is laterally discontinuous (Ma'ala et al., 1988), and yields shallow-marine fauna (gastropods, pelecypods and ostracods) (Yakta, 1976). The silty marl is greenish grey, and contains a rich fauna largely comprising large pelecypods.

The second coarsening-upward cycle also began with the deposition of a claystone bed (Unit 1), which may represent the distal part of a delta (i.e. prodelta). The siltstones and fine-grained ripple-laminated sandstones (Unit 2) may be interpreted as a distributary mouth bar at the delta front. The presence of fine-grained sandstones (Unit 3) may be interpreted as sand shoals, which formed as bars within the distributary mouth channels. Such sand shoals usually develop along the marginal parts of the channel where the velocity of the river current is lower. Fining-upward cycles within the sandstones reflect variations in depositional energy, as described by Wright and Coleman (1974).

Deposition of the overlying claystone (Unit 4) probably resulted from a renewed relative rise in sea-level, and/or a change in the location of active sedimentation. This led to the deposition of the pelecypod-rich silty marl below the M5 Marker Bed. The M5 flooding interval was followed by the restriction of water circulation in an arid to semi-arid setting, resulting in the deposition of gypsum.

Table 2: Representative X-ray fluorescence chemical analyses of sandstones from the Fatha Formation. Samples, S from Sheikh Ibrahim section and HS from Hamam Al-Alil section. Major oxides in wt%, trace elements in ppm. Total Fe as Fe_2O_3

Sample No.\ sandstone type	SiO_2	TiO_2	Al_2O_3	Fe_2O_3	MnO	MgO	CaO	Na_2O	K_2O	P_2O_5	L.O.I.	Total	Ba	Cr	Ni	Rb	Sr	V	Zn	Zr
S31 Coarse-grained red sandstone	29.12	0.32	6.45	2.53	0.10	12.48	17.14	0.6	1.49	0.07	29.06	99.13	204	231	101	41	90	457	35	75
S30 Medium-grained red sandstone	30.51	0.32	5.46	2.61	0.08	9.63	20.63	0.59	1.4	0.08	27.6	98.91	239	278	71	43	121	524	34	89
S29 Fine-grained red sandstone	37.56	0.47	7.75	3.49	0.07	3.76	16.36	0.77	1.63	0.07	27.11	98.99	331	454	133	44	241	571	39	91
HS19 Fine-grained sandstone	32.15	0.35	6.34	3.51	0.08	4.52	23.42	0.9	1.37	0.06	28.21	98.91	757	334	110	38	214	529	32	83
HS20 Coarse-grained sandstone	35.1	0.39	6.58	3.44	0.07	3.73	18.01	1	1.46	0.07	28.65	98.50	283	392	80	39	180	498	31	89
HS27 Green sandstone	32.99	0.37	7.51	3.39	0.06	3.97	22.24	0.29	1.16	0.08	27.33	99.39	123	202	159	21	529	486	40	53
HS29 Red sandstone	42.51	0.69	10.06	8.23	0.15	6.04	14.8	0.38	2.22	0.1	14.11	99.29	208	330	458	56	236	621	19	96
HS30 Red sandstone	35.53	0.58	8.35	5.23	0.10	3.65	23.24	0.75	1.37	0.1	20.08	98.98	230	177	106	35	384	654	18	110

Carbonates: Marly Limestone and Arenaceous Limestone

Carbonates generally form about 25% of the total Fatha sediments. The thicknesses of these units ranges from 0.2 to 30.0 m, with individual bed thicknesses decreasing upwards in the succession. Highly fossiliferous beds occur in the studied carbonate sections, with common shell fragments, usually recrystallized. Two main limestone lithofacies have been identified: marly and arenaceous (detrital).

Marly Limestone: yellowish grey, thinly bedded to laminated and generally fossiliferous. Internal structures are rare, but include flaser bedding, wavy laminations or domal stromatolites that alternate with arenaceous limestones. Marly limestones occupy the lower part of most carbonate horizons, but become increasingly dolomitic with a marked reduction in fossil content upwards beneath the gypsum horizons.

Arenaceous Limestone: whitish grey, visibly detrital with fossils, very hard, thinly bedded and overlain by marl and marly limestones. A shallow basin depositional setting, with salinity fluctuation from brackish through normal-to-brackish was deduced for the carbonates of the Fatha Formation based on a detailed description of ostracods by Khalaf (1994).

The organic-rich (fossiliferous) limestones are further divided into three microfacies: (1) Bioclastic-Peloidal Grainstone-Packstone, (2) Bioclastic-Peloidal Lime Mudstone-Wackestone, and (3) Lime Mudstone-Wackestone.

Bioclastic-Peloidal Grainstone-Packstone Microfacies: Several submicrofacies are distinguished according to the type and abundance of bioclasts present. Bioclasts include gastropods, rotalids, miliolids, pelecypods, bryozoans, echinoids, ostracods and calcareous algae (Figure 10). Pellets are common and vary from ovoid to sub-rounded. Ooids are also present, mostly micritized grains with a visible concentric structure. The common bladed and sparry calcite cement may be of phreatic meteoric origin (Tucker, 1993).

These sediments were deposited in a shallow-marine setting; the bioclastic-packstone was deposited on the edge of a shoal in a platform setting (Al-Hashimi and Amer, 1985).

Bioclastic-Peloidal Lime Mudstone-Wackestone Microfacies: This microfacies is characterized by fine-grained and micritic limestone with minor amounts of silt- and sand-sized grains, mainly quartz.

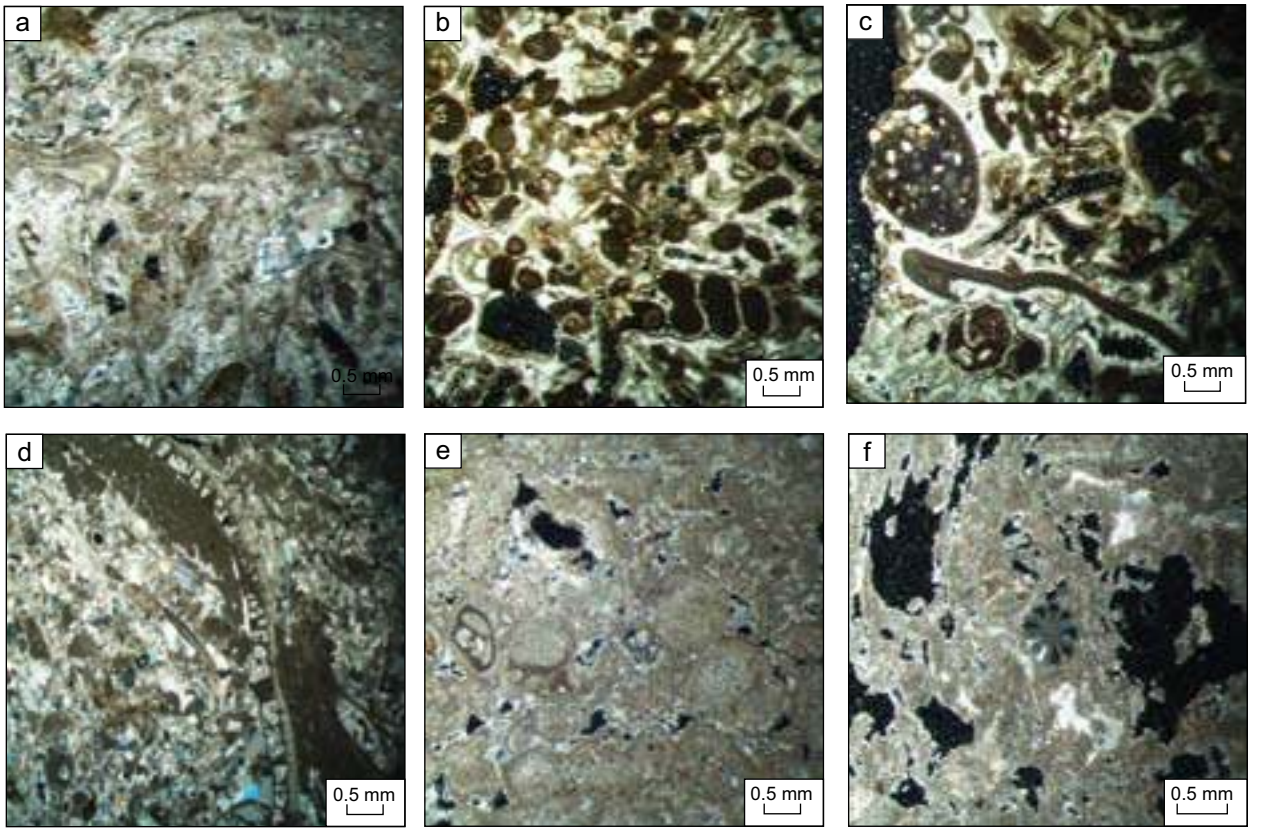

Figure 10: Photomicrographs show bioclastic-peloidal grainstone-packstone microfacies.
(a) Bryozoans, gastropods, foraminifera in drusy and bladed calcite cement; note dissolution porosity. Fossiliferous limestone, upper part of M4 in Hamam Al-Alil section (sample HS21).
(b) Gastropods, foraminifera, pellets and ooids in drusy calcite cement. Note inter and intragranular porosity due to bioclast dissolution. Cement is generally of meteoric phreatic origin, M4.
(c) Pelecypods, milliolids, bryozoans and ostracods in microsparite cement. Drusy calcite fills the cavities in bioclasts, with scattered quartz grains. Arenaceous limestone, part of M1, Hamam Al-Alil section (sample HS1).
(d) Part of pelecypod shell filled with sparry calcite in microsparite cement and scattered quartz grains, same sample as above.
(e) Pellets and ooids in microsparite cement, note interparticle porosity, with few foraminiferal remains and scattered quartz silty grains. Arenaceous limestone at Sheikh Ibrahim section (sample S12).
(f) Milliolids-rich bed with microsparite calcite cement. Limestone of M2 in Hamam Al-Alil section (sample HS10).

It occurs primarily in the upper part of the lower member. Bryozoans, gastropods, ostracods and benthic foraminifera are the common bioclasts present (Figures 11a and 11b). Peloidal (pelmicrite) microfacies with few fossil remains are noted. Generally, these pellets are ovoid and micritized with sparry calcite envelopes, sometimes dolomitized and porous (Figure 11c). Scanning electron images of these pelmicrites show the sparry calcite envelope surrounding micritic carbonates (Figure 11d). Palygorskite formed as an authigenic mineral in the voids between the pellets (Figure 11e), although euhedral dolomite crystals may also fill the voids (Figure 11f).

These sediments were deposited in quiet, shallow-water marine conditions at moderate depths and low energy.

Lime Mudstone-Wackestone Microfacies: This microfacies is fine-grained with rare ghosts of fossils. Some of the resultant voids are filled by gypsum (Figure 12a). The lime muds are generally peloidal with rare remains of ostracods, foraminifera and calcispheres. The limestone beds are characterized by a low-diversity benthic foraminifera assemblage, distinctly lacking planktonic foraminifera. Within

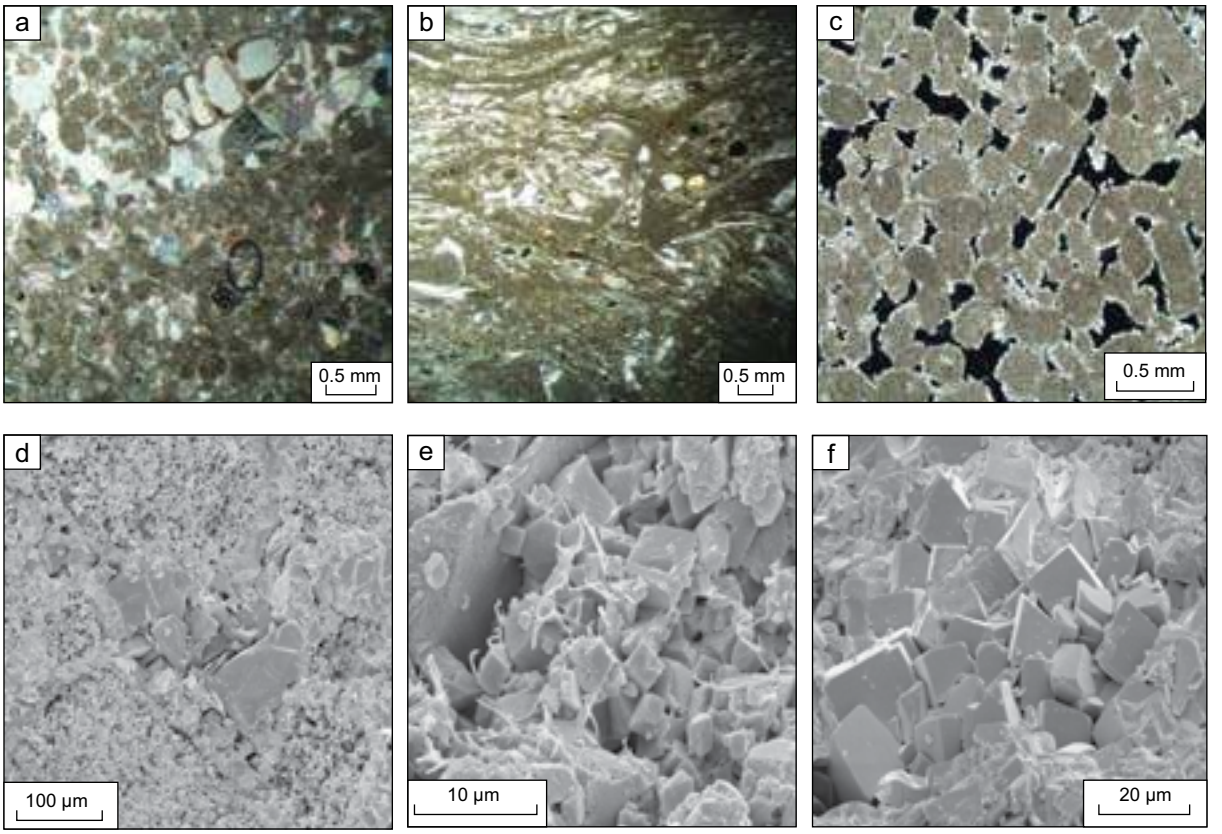

Figure 11: Photomicrographs of bioclastic-peloidal lime mudstone-wackstone microfacies.
(a) Bryozoans, gastropods and ostracods in micritic and few sparry calcite cement.
(b) Biomicrite with common scattered quartz grains. Bedded arenaceous limestone, lower part of M4, Hamam Al-Alil section (a-b, sample HS21).
(c) Pelmicrite with sparry calcite and dolomitic rims; note intergranular porosity, part of M1, Hamam Al-Alil section (sample HS1).
(d) SEM image shows sparry calcite envelope around the micritic filling of pellets, M1, Hamam Al-Alil section (sample HS1).
(e) Mixture of fine to coarse dolomite rhombs (euhedral to subhedral) and palygorskite fibers in fractures between pellets or covering dolomite rhombohedra, pelmicrites, same sample as above.
(f) Euhedral rhomb of dolomite with smooth surface filling voids and surrounding the fine (micrite) (same samples as in d).

the limestones, cryptalgal laminites, stromatolites, varied ichnofauna (including burrowers such as *Planolites* and *Skolithos*) and scavengers (such as ostracods and pelecypods) are present. SEM images show gypsum fibers and sparry calcite filling the cavities or pores in the lime mudstones (Figures 12b and 12c) with the presence of honeycomb-like palygorskite/sepiolite (Figure 12d).

These sediments were deposited in an intertidal setting, as indicated by the presence of microbial laminites (Figure 12e) and fenestral-fabric textures (Figure 12f). The presence of palygorskite as an authigenic minerals may indicate evaporitive conditions. Chamley (1989) summarized the conditions for the formation of palygorskite as alkaline in a restricted warm, humid, highly evaporative basin subject to marine transgressions providing limited water exchange.

Limestone Marker Beds: The five Limestone Marker Beds were deposited in brackish to normal marine conditions (Shawkat and Tucker, 1978). Ahmad (1980), however, concluded that some of the limestone beds were deposited in lagoonal settings. Besides the low foraminiferal diversity, she cited as evidence the presence of *Quinqueloculin*a and *Triloculina*. She confirmed that other beds were deposited in relatively shallow, tropical or subtropical marine settings, based on identifying marine

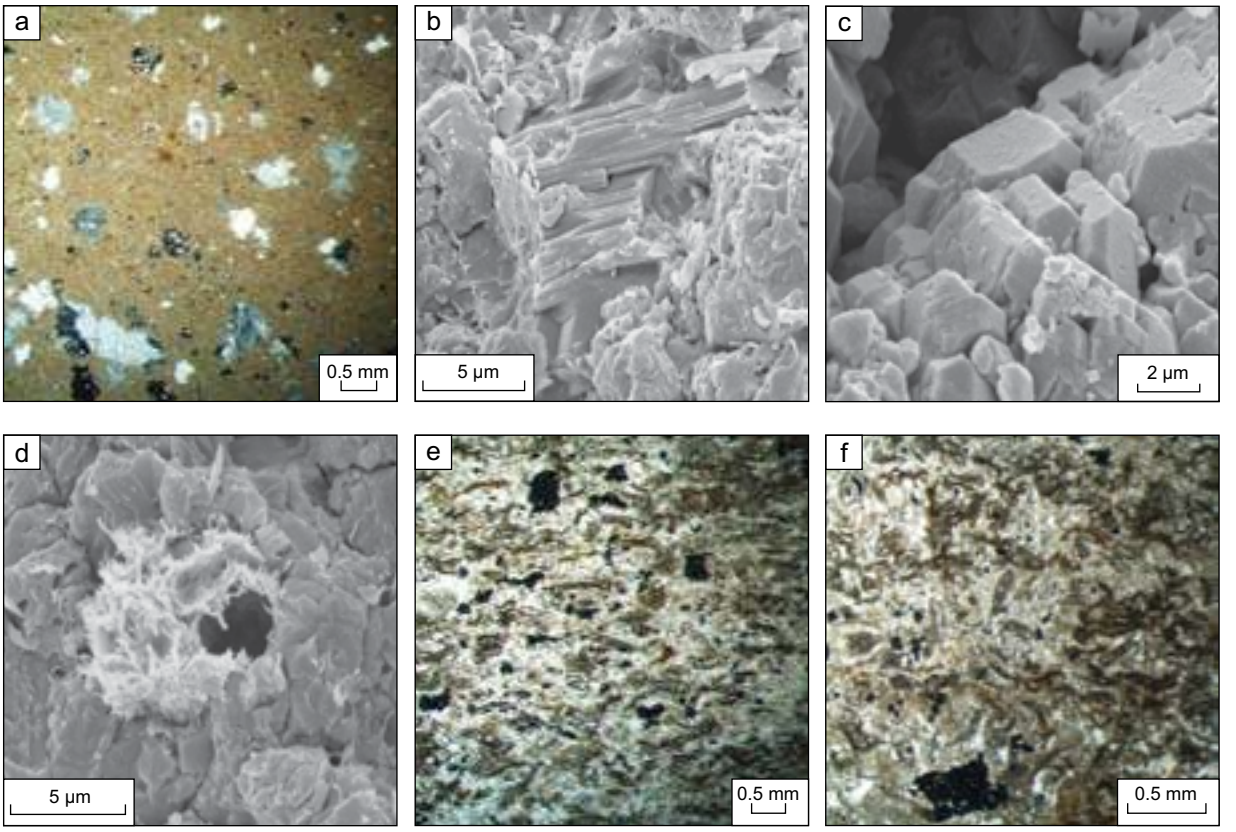

Figure 12: Photomicrographs of lime mudstone-wackestone microfacies.
(a) Gypsum and sparry calcite filling pores in micritic (lime mudstone) in Shiekh Ibrahim section (sample S20).
(b) SEM image shows gypsum fibers (centered) in pores of lime mudstone.
(c) SEM image of sparry calcite in pores of lime mudstone.
(d) Honeycomb shape of palygorskite/sepiolite filling part of the void in lime mudstone (images d to f, sample S18).
(e) Microbial laminites with few fossil remains and fenestral porosity, M3 in Hamam Al-Alil section.
(f) Enlarged view of birdseye pores in micritic to microsparry calcite; calcite fills part of foraminiferal mold. Marly limestone at Shiekh Ibrahim section (sample S20).

fossil assemblages; for example the uppermost limestone beds of the Sheikh Ibrahim section 8 and most of the limestone beds in the Maqlub and Bahzani sections (sections 6 and 7).

Carbonates: Dolomitic Limestone and Dolomite

Dolomitic Limestones: These occur mostly in the upper part of the lower Fatha Member. Some of the fine-grained dolomites are dolomicrites. They are generally porous (Figure 13a) with an MgO content reaching 16.0% (Table 3). Some of these dolomicrites are crystallized, either partly or completely, into sucrosic dolomite (Figures 13b and 13c). SEM images show fine, clayey, aphano-crystalline to coarse crystalline dolomite (Figure 13d), with the presence of palygorskite and gypsum fibers and plates in the pores between the dolomite rhombs (Figures 13e and 13f). Fossil traces are also obvious (Figure 13g), as is evidence of burrowing (Figure 13h). Some dolomitic limestones contain strontium in higher amounts. These rocks mostly occur at the basal contact of the Fatha Formation with the underlying Jeribe Formation and are intercalated with yellow micrite and marly limestones.

Dolomite: usually associated with gypsum and aragonite. The presence of aragonite is confirmed by XRD analysis (Figure 14) and SEM images (Figure 15). Aragonite is present as elongate fibers, composed of euhedral crystals with non-porous growth. This type of aragonite can be termed

botryoidal aragonite, and is similar to Miocene aragonites of the Red Sea (Aissaoui, 1985). It forms on a fixed substrate and exhibits a fan structure (Figures 15a and 15b). The crystal form may be rounded to ovate with angular crystal ends and a cone shape generally oriented normal to the substrate (Figures 15c and 15d). This type of aragonite may precipitate in marine as well as non-marine environments. Dry conditions favour the preservation of aragonite, while the transformation of aragonite to calcite and the dolomitization of aragonite are diagenetic processes occurring through dissolution and reprecipitation. The aragonite in the present study may be a surficial weathering feature. In general, dolomitization affects the lower part of the formation and is believed to be an early syndepositional process resulting from hypersaline conditions.

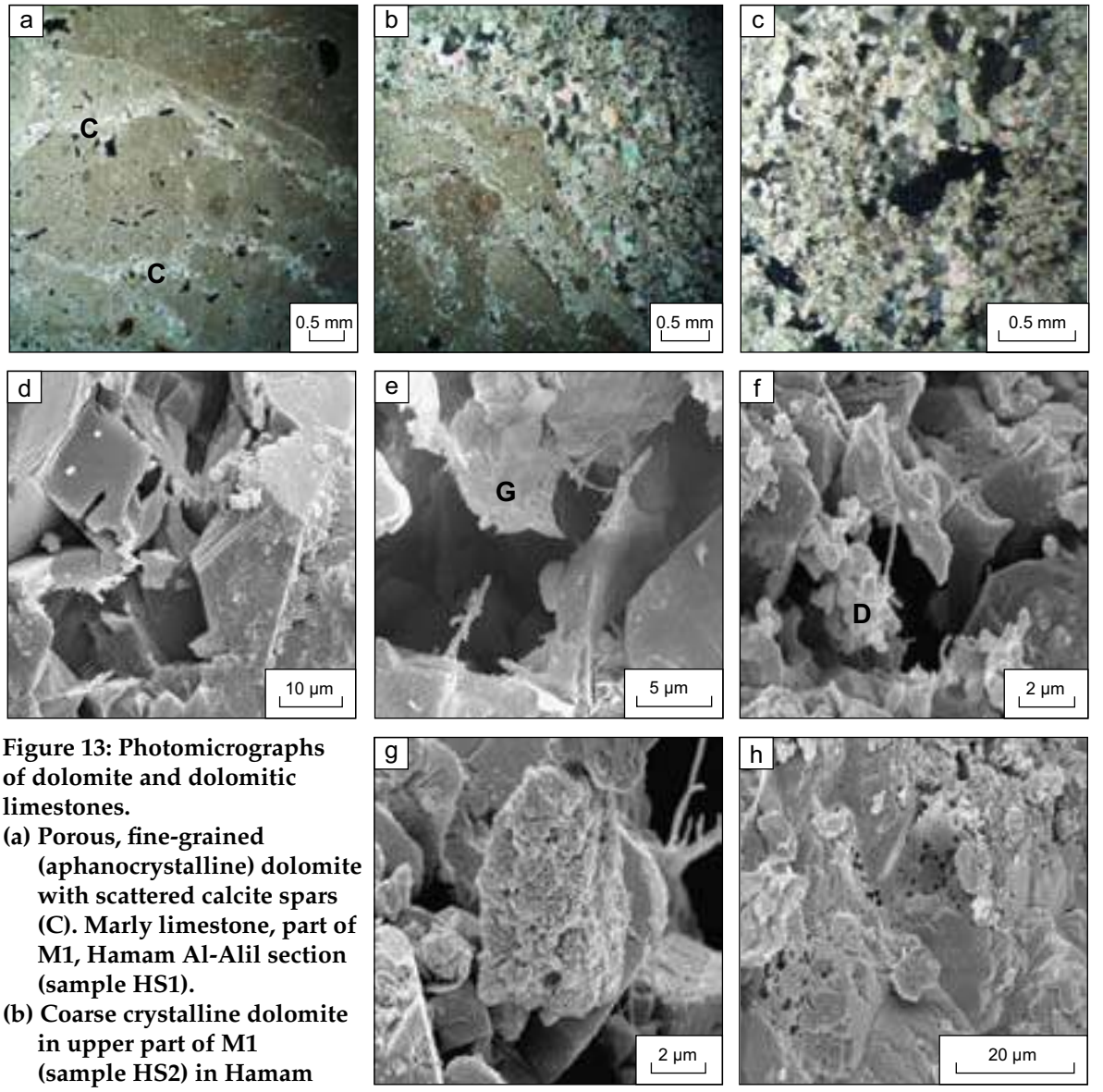

Figure 13: Photomicrographs of dolomite and dolomitic limestones.
(a) Porous, fine-grained (aphanocrystalline) dolomite with scattered calcite spars (C). Marly limestone, part of M1, Hamam Al-Alil section (sample HS1).
(b) Coarse crystalline dolomite in upper part of M1 (sample HS2) in Hamam Al-Alil section; note partial dolomitization of the bed.
(c) Coarse crystalline to sucrose dolomite, Hamam Al-Alil section (sample HS3).
(d) SEM image of aphanocrystalline to coarse crystalline dolomite.
(e and f) SEM images of palygorskite fibers in cavities of dolomite with few gypsum plates (G) in dolomitic limestones; note dolomite rhombs (D). Images d to f from Hamam Al-Alil section (sample HS14).
(g) Remains of fossil (centered) in dolomitic limestones at Sheikh Ibrahim section (sample S3).
(h) Burrowing in dolomitic limestone with few scattered calcite grains, same sample as above.

Depositional Setting

The basal part of the Fatha Formation was deposited in a barred hypersaline lagoonal environment. The above characteristics suggest that evaporative dolomitization occured in a tidal-flat setting, where microbial mats were common. Intensive dolomitization occurs in mud-dominated sediments associated with evaporites of the capping sabkha-lagoonal sequence of the Miocene (Euphrates and Jeribe formations) of the Mesopotamian Basin (Sun, 1995). The presence of aragonite as small fibers (Figure 15), in addition to dolomitization in evaporitic conditions and mixed water conditions with elevated temperatures, may have been responsible for the higher amount of strontium in these rocks (Kinbell and Humphrey, 1994).

Table 3: Geochemical analysis of the different types of limestone from the Fatha Formation. Major oxides in wt%, trace elements in ppm.

Sample No.	Type of Limestone	SiO_2	Al_2O_3	MnO	MgO	Na_2O	CaO	K_2O	TiO_2	P_2O_5	Fe_2O_3	L.O.I.	Total	Ba	Sr
HS9	Marly	2.51	0.68	0.04	5.42	0.15	45.66	0.10	0.04	0.04	0.37	40.86	95.97	64	274
S20		2.55	0.65	0.03	0.68	0.14	50.03	0.09	0.04	0.04	0.24	40.53	95.02	16	329
HS1	Dolomitic	3.56	0.90	0.01	15.95	0.30	33.37	0.16	0.05	0.03	0.24	40.63	95.20	6	248
S3		2.58	0.83	0.01	15.15	0.15	33.41	0.12	0.05	0.05	0.15	42.83	95.33	65	2935
S8		5.89	1.48	0.02	16.92	0.12	31.67	0.30	0.10	0.08	0.71	39.65	96.94	28	98
S24		2.46	0.68	0.02	14.02	0.19	30.59	0.12	0.04	0.05	0.01	44.83	93.01	12	146
HS21	Crystalline	1.53	0.47	0.01	0.58	0.17	51.84	0.02	0.03	0.04	0.05	40.36	95.10	4	554
HS12	Fossiliferous	3.54	1.03	0.04	6.97	0.16	44.79	0.15	0.05	0.04	0.5	40.52	97.34	23	219
HS3	Arenaceous	5.69	1.47	0.10	13.81	0.24	35.64	0.35	0.09	0.06	0.94	39.44	97.83	125	262
HS18		25.8	5.35	0.11	1.99	0.76	28.19	0.11	0.39	0.07	2.88	33.64	98.57	148	233
S12		14.16	3.47	0.03	15.96	0.14	24.60	0.94	0.23	0.11	1.98	36.45	98.19	65	203

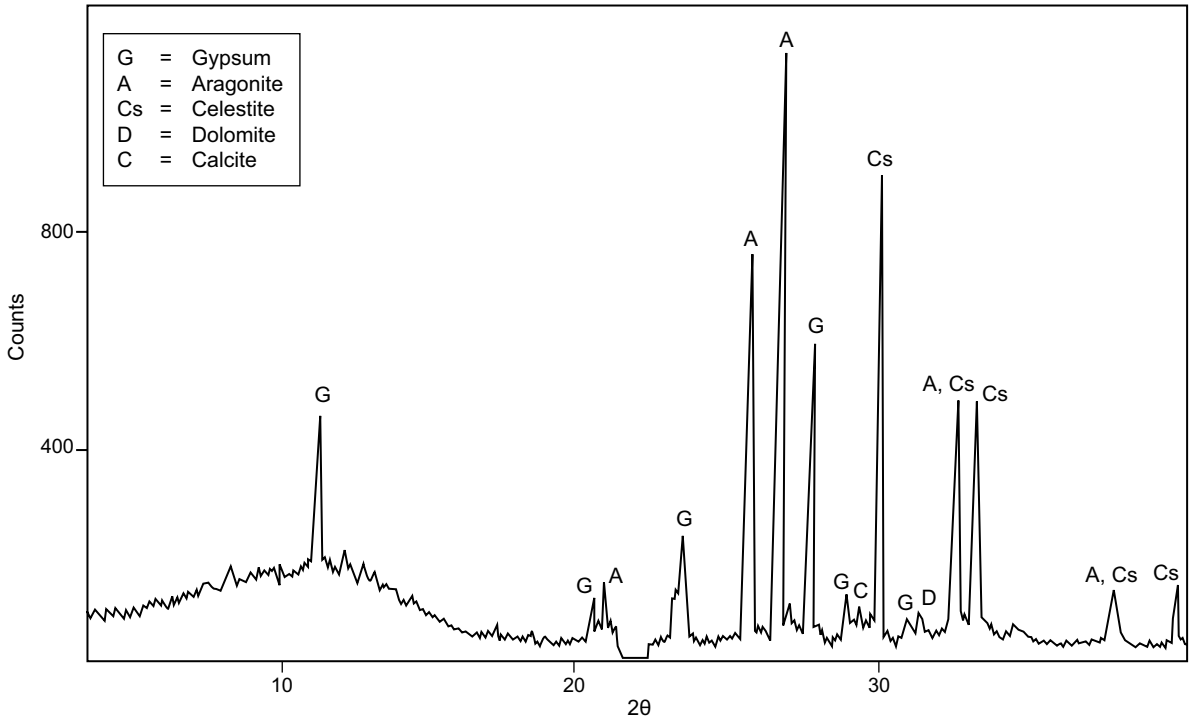

Figure 14: X-ray diffractogram of aragonite sample containing aragonite, gypsum and celestite (Hamam Al-Alil area, sample HS14).

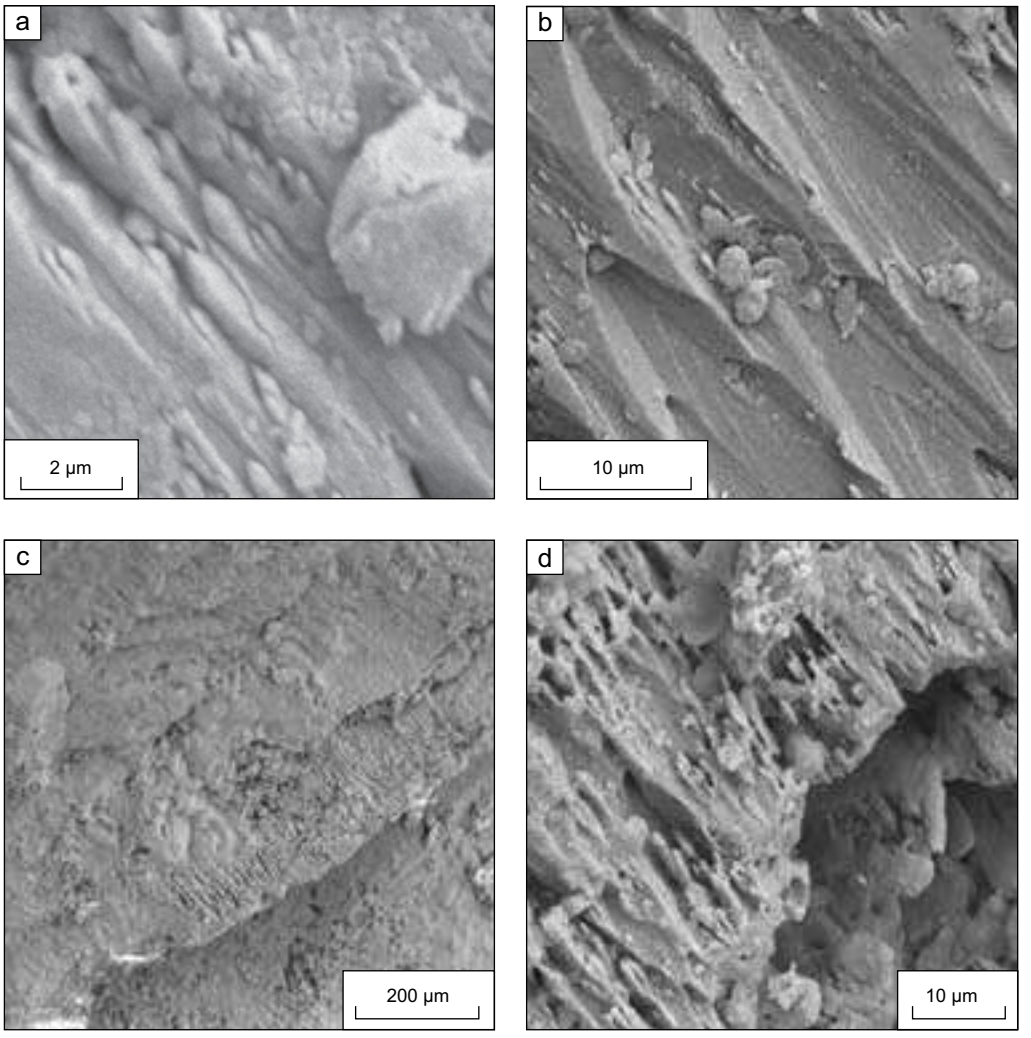

Figure 15: SEM images of aragonite.
(a) Radial shape of aragonite directly oriented to the substratum.
(b) Enlarged view for part of (a) showing fan-shaped structure of the substratum.
(c) Radial nature of aragonite growth, same sample as above.
(d) Enlarged view of (c) illustrates this directional radial growth, (sample HS14).

The coexistence of palygorskite fibers with dolomite reflects lagoonal, brackish-hypersaline, alkaline waters and magnesium-rich environments that were suitable for authigenic formation of this mineral. Seasonably arid climatic conditions, in the absence of local tectonic activity, promoted elevated salinity and intense evaporation, which in turn supported the direct chemical precipitation of palygorskite. The honeycomb-like morphology of the palygorskite that fills the cavities in the dolomite is attributed to a late-stage dissolution of dolomite. This process released magnesium and led to palygorskite precipitation when excess silica became available from the transformation of clay minerals in the interbedded mudrock.

Evaporites

Sulphates form about 50% of the total thickness of the formation, with beds ranging in thickness from 0.1 to 30.0 m. In surface outcrops, gypsum is the most common type of sulphate, while in subsurface sections, anhydrite and halite are the most common evaporites. Nodular gypsum is the dominant gypsum type, although laminated and thick-bedded gypsum are also present. Nodular gypsum passes gradually and vertically into thick to very thick-bedded gypsum. Secondary gypsum (selenite and satin spar) also occurs.

Table 4: Geochemical analysis of the different gypsum types of the Fatha Formation. (HS= samples from Hamam Al-Alil area; S, from Sheikh Ibrahim area). Major oxides in wt%, trace elements in ppm.

Sample No.	Gypsum type	SiO_2	Al_2O_3	MnO	MgO	Na_2O	CaO	K_2O	TiO_2	P_2O_5	Fe_2O_3	SO_3	L.O.I.	Total	Ba	Sr
S4	Nodular	1.38	0.40	0.01	0.21	0.10	17.96	0.01	0.02	0.03	0.02	47.81	30.72	98.85	2.81	246.3
HS4	Laminated	3.06	0.94	0.01	1.91	0.13	19.51	0.08	0.03	0.03	0.13	46.11	27.51	99.58	1.38	109.9
HS13	Thick-bedded	1.59	0.48	0.01	0.40	0.14	18.23	0.01	0.02	0.03	0.02	47.53	29.81	98.27	0.56	244.7
HS23	Nodular	1.76	1.34	0.01	0.26	0.08	18.45	0.01	0.03	0.03	0.03	46.81	30.32	99.13	4.58	614.9
S17	Thick-bedded	2.22	0.66	0.01	0.71	0.17	18.18	0.02	0.03	0.03	0.04	47.62	28.56	98.23	4.49	200.7
S11	Laminated	2.95	0.88	0.01	1.82	0.12	19.01	0.07	0.03	0.03	0.11	45.81	27.45	98.29	1.22	112.6
S16	Selenite	2.38	0.72	0.01	0.67	0.15	18.63	0.03	0.03	0.03	0.05	47.92	28.73	99.35	1.84	83.3

The gypsum is white and sugary or creamy in colour, although red, pink and greenish white varieties are also present. The greenish white colour is usually related to secondary coloration resulting from the presence of an enveloping cover of marl. The chemical compositions of selected nodular, laminated and secondary (selenite) gypsum samples are presented in Table 4.

Nodular Gypsum

Gypsum nodules are irregular, cylindrical or spheroidal and vary in length from 0.5–20.0 cm. The nodules are aligned perpendicular to the bedding plane and gradually become equi-dimensional or flattened in an upward direction. Generally, the nodules are free of inclusions and are composed of very fine, sugary, compacted and alabastrine material. Each nodule is coated, either completely or partially, by a film of grey calcareous sediments. These nodules are classified into five categories: compound mosaic, compound wispy, mosaic, wispy and structureless forms. Petrographically, nodular gypsum is formed from granular integrated gypsum with some evidence of recrystallization (Figure 16a).

Depositional Setting: The deposition of nodular gypsum may represent a very shallow, arid, semi-restricted marine environment that underwent reflux and influx processes. Shawkat and Tucker (1978) concluded that the gypsum beds represent deposition in a sabkha or supratidal flat setting; a coastal or inland sabkha with a semi-barred, shallow lagoon has also been suggested (Mustafa, 1980). Semi-restricted lagoonal environments, such as lakes, connected to the open sea through narrow channels coincide with the "brine filled basin model" suggested by Sulayman (1990) for gypsum deposition in the Butma West area (section 4 of the present study).

Laminated (Alabastrine) Gypsum

This type of gypsum deposit is less common than other varieties. It consists of alabastrine-type gypsum, laminated (either horizontally or wavy) and separated by a green-grey calcareous film of sediments. Occasionally laminae of selenite and satin-spar are sandwiched between the laminated carbonate and alabastrine gypsum. Petrographically, this shows alabastrine fine to coarse fibrous gypsum and porphyroblastic textures (Figures 16b and 16c), with the alabastrine type predominating.

Depositional Setting: Laminated gypsum may represent pulses of sea-water influx into the Fatha Basin, which could also have led to the precipitation of a thin film of calcareous sediments. The alabastrine secondary gypsum (granular and fibrous) and porphyroblastic gypsum indicate that the gypsum is of secondary origin formed by the transformation of the pre-existing anhydrite on or near the surface by hydration.

Selenite and Satin-Spar

Secondary gypsum forms as veins or lenses of selenite or satin-spar and usually occurs in fractures or vugs and bedding planes of bedded gypsum and carbonates. Selenite is characterized by its foliated

nature (Figures 16d to 16f), which cleaves into several colourless and transparent, cleavage folious sheets. It occurs either as veins, clusters or rosettes growing within the vugs of a massive gypsum body. It occasionally occurs as dark inclusions, as small nodules randomly distributed within a mosaic gypsum. Satin-spar forms as fibrous and silky gypsum. The lengths of individual crystals range from microscopic up to 40 cm. They usually take the shapes of fractures, vugs or bedding planes and follow the boundaries of nodules.

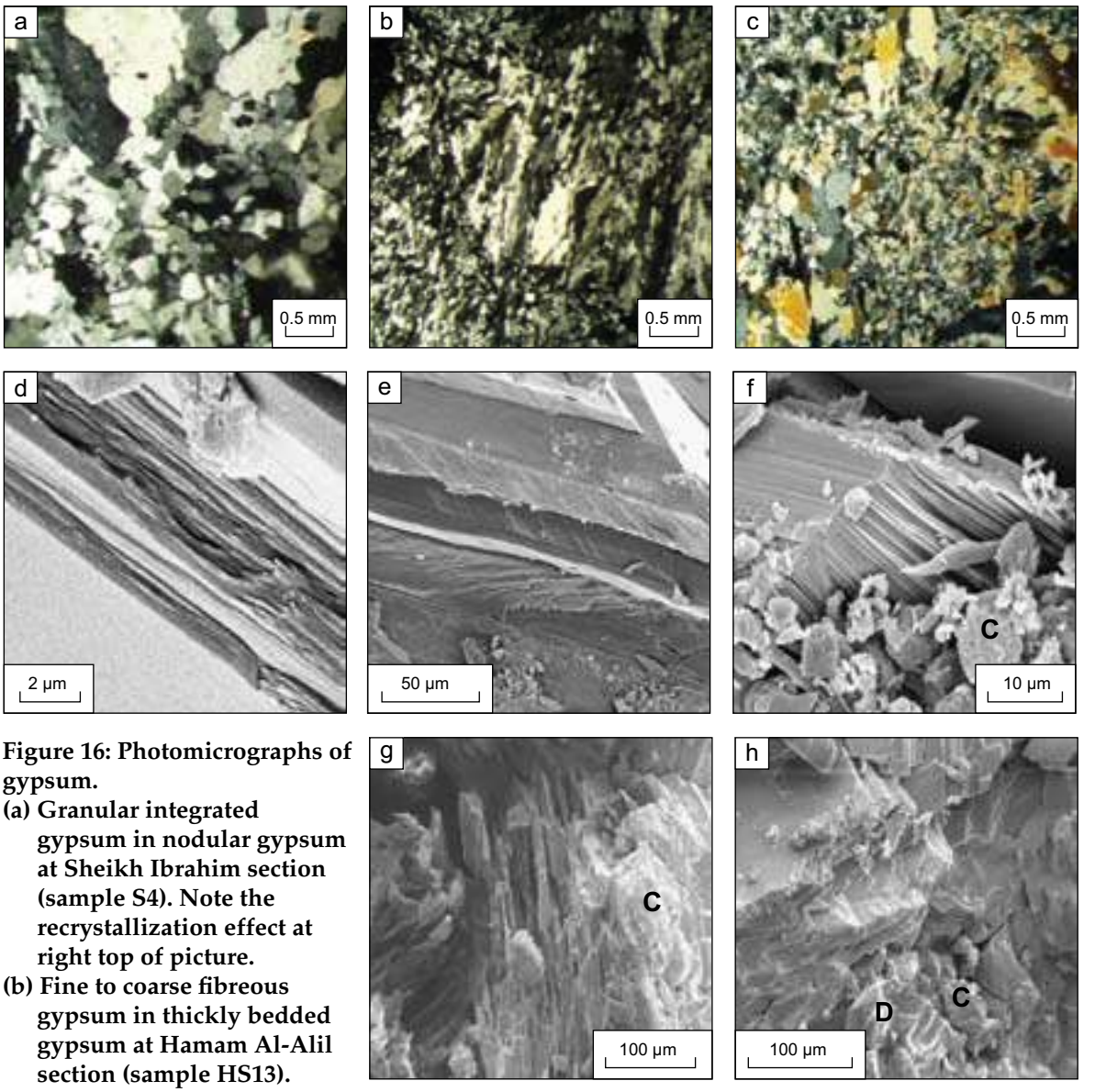

Figure 16: Photomicrographs of gypsum.

(a) Granular integrated gypsum in nodular gypsum at Sheikh Ibrahim section (sample S4). Note the recrystallization effect at right top of picture.

(b) Fine to coarse fibreous gypsum in thickly bedded gypsum at Hamam Al-Alil section (sample HS13).

(c) Porphyroblastic gypsum in thickly bedded gypsum at Sheikh Ibrahim section.

(d) SEM image shows alternating white and dark folia in selenitic gypsum at Sheikh Ibrahim section (sample S16); note obvious fractures in the dark folias with scattered carbonate fragments.

(e) Foliated nature of selenitic gypsum.

(f) Broken folias of selenite with carbonate inclusions (C), same sample as (d and e).

(g) Coarse crystalline gypsum with scattered fine calcite; note some of the carbonates (C) present in a band that may be responsible for the grey color of the gypsum.

(h) Fibreous gypsum with scattered carbonates as dolomite rhombs (D) and fine calcite (C) in bedded gypsum, (sample S11).

Depositional Setting: Secondary gypsum (selenite and satin-spar) may have formed by the transformation of anhydrite into gypsum. Petrographic investigation of subsurface anhydrites of the Fatha Formation by Al-Marsoumi (1980) indicated that these anhydrites are of secondary origin, and mainly comprise the 'Epigenetic Anhydrite' type with two varieties: a felty type of fibrous form and bacillar type of rhombic and spindle shapes. Recrystallization of anhydrite took place under stress by an overburden load that caused the formation of flowage structures, compound grains, parallel elongation of crystals and crystal coalescence (Al-Marsoumi, 1980).

Figures 16g and 16h show the different types of gypsum as fine- to coarse-crystalline fibrous, in addition to the presence of dolomite rhombs, which form the dark bands in some of the gypsum nodules. Mineralogical investigation by XRD showed that the rocks mainly consist of gypsum with smaller amounts of dolomite (Figure 17). In contrast, the study of gypsum samples from the Butma West area by Sulayman (1990) showed that the gypsum rocks there also contained small percentages of anhydrite, celestite, quartz and bassanite.

The lower values for strontium in the secondary selenitic and laminated gypsum (Table 4) may be related to its partial expulsion by hydration from the original anhydrite. The impoverishment of strontium in these types of gypsum (compared to the primary studied gypsum) is consistent with the ideas of Playa et al. (2000) for the origin of fabrics in the Upper Miocene evaporites in the Eastern Betics. The gypsum samples also contain higher MgO%, which may be attributed to diagenetic processes and salinity. The presence of dolomite rhombs and sparry calcite in the gypsum (Figure 16h) may cause the high magnesium content in this gypsum. The geochemical behavior of strontium and magnesium is a good criterion for indicating the diagenetic stages of gypsum deposit formation (Fort and Bustillo, 1986).

Halite

Halite occurs only in the subsurface sections; these are concentrated in the center of the depositional basin (Dunnington, 1968) and are generally surrounded by units dominated by anhydrite beds (Stöcklin, 1968). The thickness of the halites varies considerably due to diapirism (van Bellen et al., 1959). Tucker (1999) reported that the halite is well-bedded, with occasional thin layers (5.0–20.0 cm) interbedded with thin clay stringers. These may also occur as alternations of clay-rich and clay-poor halite, which were deposited either in shallow subaqueous lakes or in salinas and salt pans.

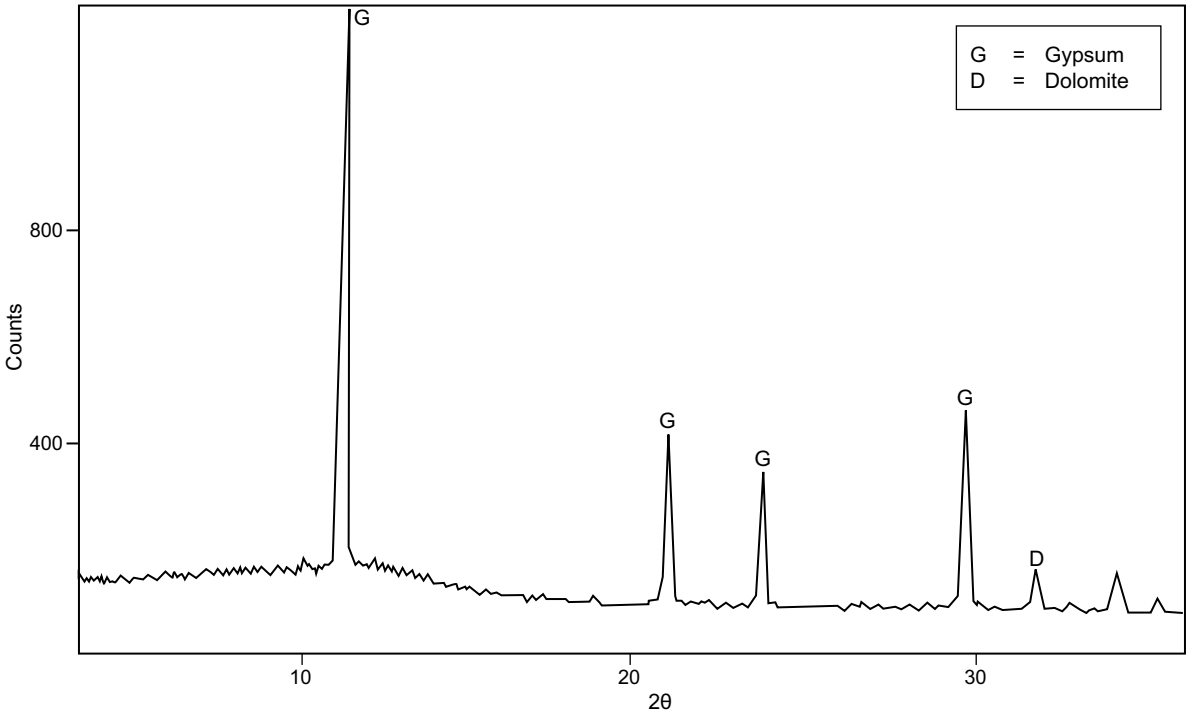

Figure 17: X-ray diffractogram of nodular gypsum sample from the Fatha Formation in Sheikh Ibrahim area (sample S4).

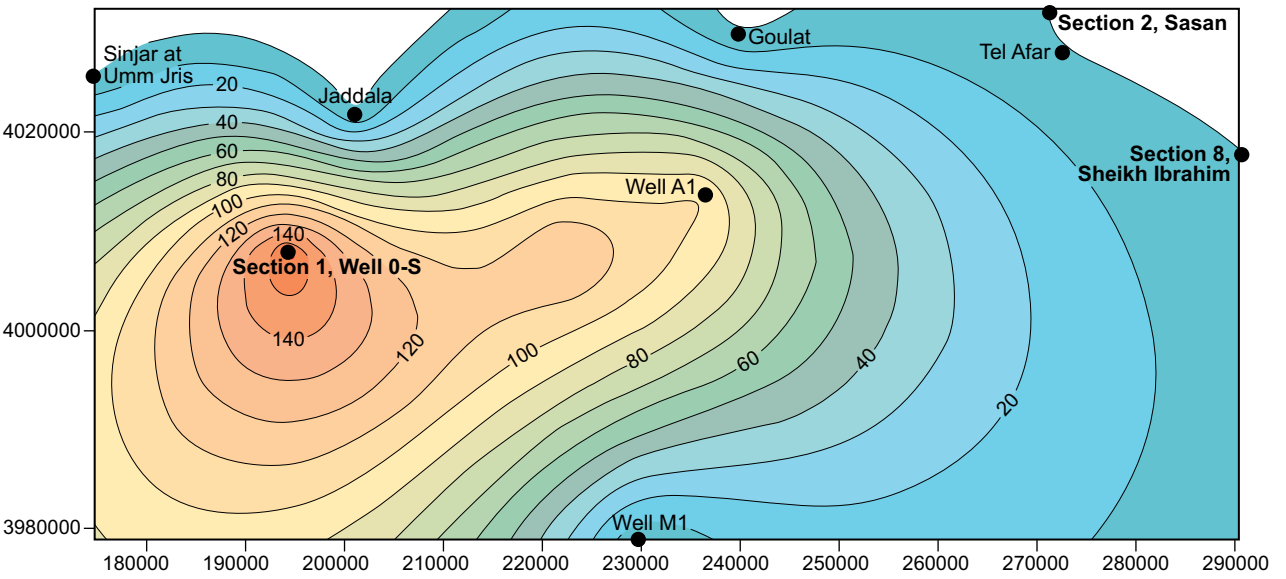

Figure 18: Isopach thickness map of halite in part of Sinjar Basin (coordinations in UTM), locations: sections from the present work are Section 1, Well 0-S; Section 2, Sasan; and Section 8, Sheikh Ibrahim. Other sections are used for comparison (Sinjar at Umm Jris; Jaddala; Goulat; Tel Afar; Well M1; and Well A1).

The distribution of lithofacies of the Fatha Formation in both basins (Figure 3) reflects facies zonation around the halite-rich basin center. An isopach map of the halite thickness in the Sinjar Basin (Figure 18) shows this zonation, which is attributed to the palaeosalinity gradient within the basin as a function of the solubility of salt. Many salt basins share a common palaeogeography, in which a lake is separated from the sea or ocean by a narrow barrier, and the salt was mostly deposited in the basin center. Example of these basins are the Aptian evaporites of the south Atlantic rift basin, the Messinian salt deposits of the Mediterranean sea and the North Caspian depression (Nunn and Harris, 2007).

CHRONO-SEQUENCE STRATIGRAPHY

Regional Setting

In the Late Cretaceous, the Neo-Tethys Ocean began to close, as is evident by the obduction of ophiolites in Oman and elsewhere along the margin of the Arabian Plate (e.g. Beydoun, 1991; Sharland et al., 2001; Searle, 2007). By the Late Miocene and Early Pliocene, the Neo-Tethys Ocean closed by the collision of the Arabian and Eurasian plates (Central Iran and Turkey), and the Zagros and Taurus Mountain belts started to be uplifted (e.g. Buday and Jassim, 1987; Al-Sharhan and Nairn, 1997). Between these two tectonic events, starting in the Late Eocene and continuing through the Middle Miocene, crustal loading and flexure of the eastern Arabian Plate formed the broad and shallow Mesopotamian Basin as a NW-oriented foreland basin (Jordan, 1981; Allen et al., 1986). This 2,000-km-long basin extended from Bandar Abbas, in Iran, across Iraq and Syria to the Mediterranean Sea, and was located southwest of the Zagros and Taurus Mountains (Figure 1).

In the Mosul area in northern Iraq, an uplifted regional trend was probably structurally active during the deposition of the Fatha Formation (*Mosul High* of Numan, 1984); it affected the development of accomodation space and the distribution of sediments. This is evident by the decrease in thickness of the Fatha carbonates away from the structural high, and their facies change from bioclastic limestones (with abundant oyster shell fragments) to dolomitized micrite. It is also evident from the increased thickness of the evaporites (and associated salt) towards Sinjar (Jassim et al., 1997).

In greater structural detail, two major uplifted blocks are recognized: the NW-trending Kirkuk and E-W trending Mosul structural blocks. The Kirkuk and Mosul blocks run parallel to the Zagros Suture and Taurus Mountains, respectively. The change between their trends occurs along the Greater Zab

River. The two blocks themselves consist of smaller fault blocks of varying sizes, which also affected the sedimentary facies and thickness changes of individual formations.

Based on the distribution of lithofacies data (Mustafa, 1980; Jassim and Karim, 1984), the study area can be divided into two basins separated by a palaeoridge. The western *Sinjar Basin* (includes sections 1-8) extends into Syria; it is fragmented into smaller sub-basins (e.g. the Butma sub-basin), as shown by the increased thicknesses of the Fatha Formation in the Butma West area (sections 3 and 4, Figure 3a). The eastern *Kirkuk Basin* (includes sections 9-12, Figure 3b, also *Fatha Basin*) extends southeast into Iran.

Although tectonic activity was responsible for the formation of the foreland basins, the associated structural processes occurred on a much longer time scale (c. 10 million years) compared to the duration of the high-frequency Fatha eustatic cylicity (c. 10s to 100s thousand years). The Fatha Formation was deposited in a frequently flooded, semi-restricted evaporitic foreland basin subjected to high evaporation due to aridity. The sea encroached on the basin from the Mediterranean Sea in the west and the Neo-Tethys Ocean in the southeast. The shoreline ran from Haditha to Abu Jir, Najaf, Samawa, then swung slightly to the south towards the Iraqi-Kuwaiti-Saudi Arabian border junction (Figure 1).

Sequence Boundaries

In northern Iraq, the Basal Fatha Conglomerate represents a regional transgression over the eroded Eocene Pila Spi Limestone or Avanah Limestone formations (van Bellen et al., 1959). In the Fars Basin, the conglomerate is absent, and the Fatha Formation conformably overlies the Lower Miocene Jeribe Formation (van Bellen et al., 1959). These relatonships indicate that the base of the Fatha Formation changes from an unconformity at the edge of the basin to a correlative conformity within it; i.e. it is a sequence boundary. The top of the Fatha Formation, marked by Upper Red Beds and terminal A0 Anhydrite, suggests that the Injana/Fatha contact is also a sequence boundary.

Global and Arabian Plate Sequence Stratigraphy

Figure 19 compares various chrono and sequence stratigraphic interpretations of the Fatha Formation and bounding units. Figure 19a shows the age assignments and regional correlations from James and Wynd (1965). Goff et al. (1995, Figure 19b) combined the Middle and Lower Fars formations in northern Iraq into their Sequence 3.2 of early Middle Miocene age. They correlated their Sequence 3.2 to Sequence TB2.5 of Haq et al. (1987) (planktonic foraminiferal zones N11 and lower N12; Late Langhian). They interpreted the underlying Jeribe Formation as Sequence 3.1 of earliest Middle Miocene age and correlated it to Sequence TB2.4 of Haq et al. (1987) (planktonic foraminiferal zones N9 and N10; early Langhian).

Sharland et al., (2001, 2004, Figure 19c), following van Bellen et al. (1959), interpreted four Arabian Plate maximum flooding surfaces (MFS) in the Miocene; their ages in million years (Ma) were revised by Simmons et al. (2007):

MFS Ng40 (14.5 Ma): Middle Miocene, Late Langhian, marine carbonates of the Middle Fars Formation (= lowermost Upper Fars Formation) (van Bellen et al., 1959); here Injana Formation.

MFS Ng30 (15.9 Ma): Middle Miocene, Early Langhian, marine carbonate near base of Lower Fars Formation (van Bellen et al., 1959); here Fatha Formation.

MFS Ng20 (17.5 Ma): Early Miocene, Late Burdigalian, carbonates near the base of the Jeribe Formation (van Bellen et al., 1959).

MFS Ng10 (20.0 Ma): Early Miocene, Early Burdigalian, carbonates near the base of the Euphrates Formation or equivalent Serikagni Formation (van Bellen et al., 1959).

Jassim and Buday (2006, Figure 19d) interpreted the Fatha Formation as Early Miocene in age.

The Fatha Formation forms a transgressive-regressive third-order sequence bounded by two sequence boundaries.

(a)

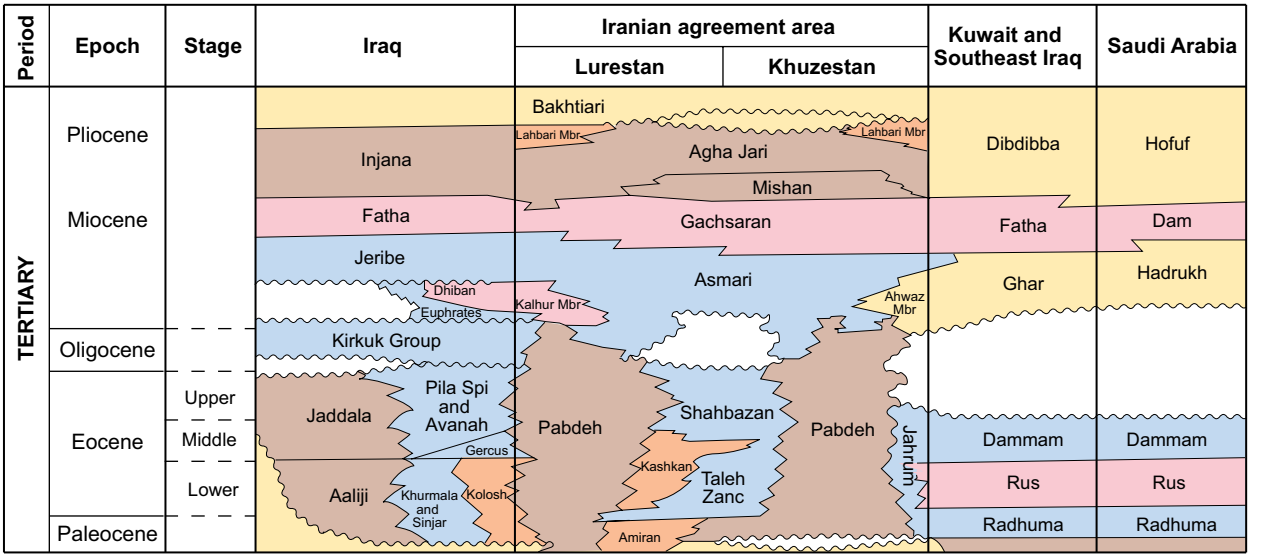

(b)

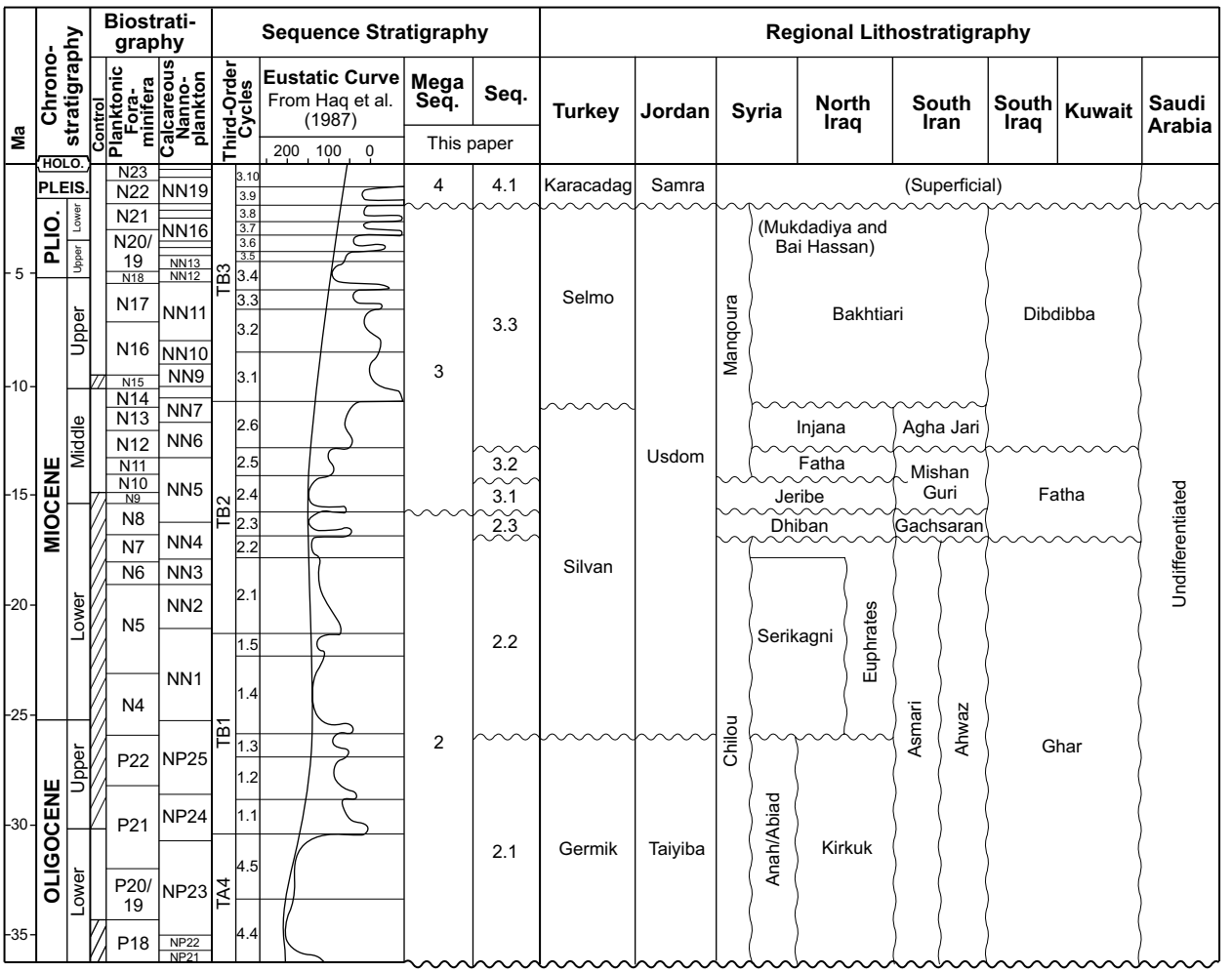

Figure 19: (a) Regional correlation between the Tertiary formations in Syria, Iraq, Iran, Kuwait and Saudi Arabia (after James and Wynd, 1965).
(b) Regional correlation in the Middle East by Goff et al. (1995) based on Haq et al. (1987).
See facing page for continuation.

(c)

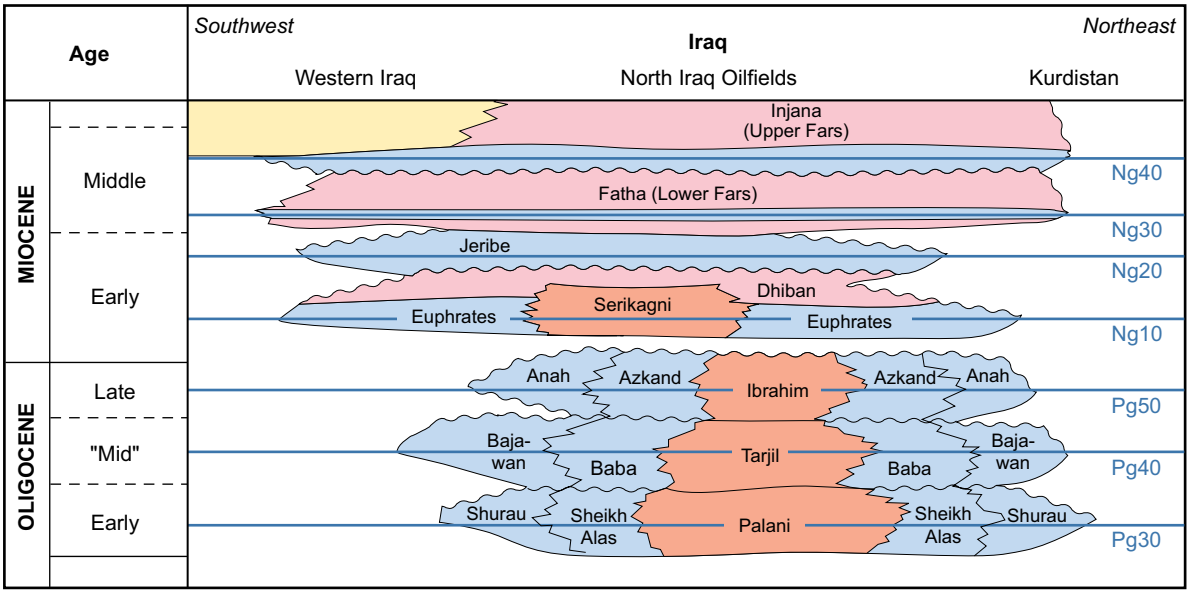

(d)

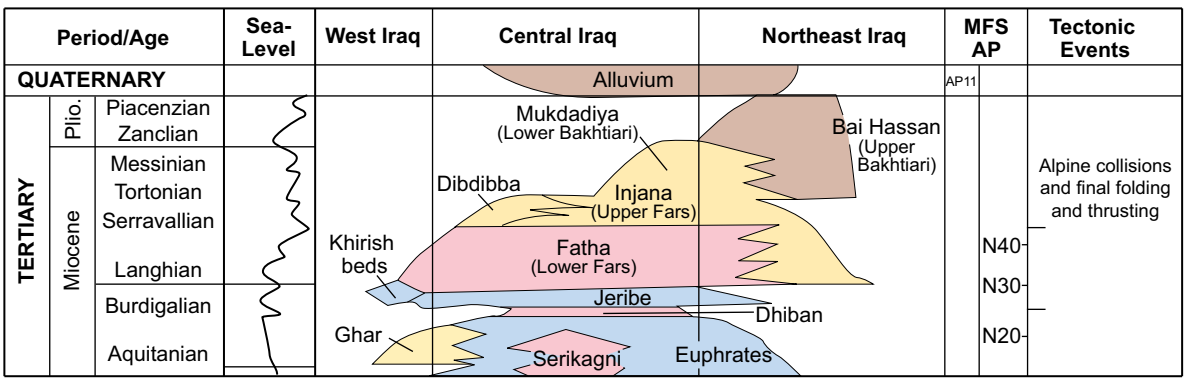

Figure 19 (Continued): (c) Interpretations for Iraq by Sharland et al. (2001, 2004). The contact between Oligocene and Miocene is modified after Al-Banna (2008).
(d) Jassim and Buday (2006). In the present study, the Fatha Formation is interpreted as a third-order depositional sequence of Middle Miocene (probable Langhian) age.

Age of the Fatha Formation: Middle Miocene, Langhian?

The age of the Fatha Formation is not resolved by biostratigraphy. It has been interpreted as "Middle Miocene" (van Bellen et al., 1959; Goff et al., 1995; Sharland et al., 2001; Jassim and Buday, 2006), and more specifically Serravallian (Prazak, 1978; Jones and Racey, 1994). In Iran, the base of the Gachsaran Formation, considered equivalent to the Fatha Formation, in southern Iraq (Goff et al., 1995), has been dated by strontium isotopes as Early Miocene, Mid-Burdigalian (Ehrenberg et al., 2007). Jassim and Buday (2006) attribute to Ponikarov et al. (1967) a Late Miocene (Tortonian) age interpretation for the correlative Lower Fars Formation in Syria. Sharland et al. (2004) followed Adams (1992) in considering *Miogypsina* to represent global planktonic zone N8 or N9, and therefore positioned the Lower Langhian maximum flooding surface MFS Ng30 in the lower carbonates near the base of the Fatha Formation.

Higher-order Parasequences

The Fatha Formation is characterized by high-frequency cycles consisting of alternating greenish grey and reddish brown marls and flooding limestones, capped by gypsum and/or anhydrite and halite (salt). Thin marly limestone beds at the beginning of each cycle represent high-frequency marine

transgressions. Subsequent evaporation initiated a phase of regression, leading to the development of extensive supratidal sabkhas, in which nodular gypsum and/or anhydrites dominate. Thin evaporites dominate the basin margins and are associated with red claystones and litharenites. Halite deposition in the basin center represents the final remnants of the shrinking sea in salinas or salt pans.

The cyclic deposition of carbonates, evaporites and siliciclastics indicates frequent flooding followed by restriction and continental exposure. Similar cyclicity occurred in the partly coeval Gachsaran Formation of Iran (Gill and Ala, 1972). The cyclicity is comparable to similar deposition of the Messinian basins of the Mediterranean Sea (Rouchy et al., 1998; Roveri et al., 2003) and to the Middle Miocene (Badenian) basin-margin evaporites of the Carpathian Foredeep Basin of western Ukraine (Peryt, 2001).

ECONOMIC SIGNIFICANCE

Northern Iraq, especially the Kirkuk Basin, contains one of the most prolific petroleum systems in the Middle East (Goff et al., 1995). The basin is highly structured; its anticlines house giant and supergiant oilfields containing several stacked source-reservoir-seal triplets (e.g. Euphrates-Dhiban Anhydrite, Jeribe and Fatha formations; Al-Juboury et al., 2007). The Fatha evaporites provide the uppermost regional seal for the Miocene reservoirs in the Zagros foreland fold belt in Iraq (Goff et al., 1995). Most of the sub-salt accumulations are structurally and broadly-drained anticlinal culminations. This demonstrates the ability of the evaporites to maintain seal-integrity under deformation, while the underlying and intercalated dolomites and limestone became fractured (Warren, 2006).

The Fatha Formation has been identified as a reservoir in eleven structures, mostly in southeastern and southern Iraq (Aqrawi, 1993). It also contains oil and gas in many oilfields in central Iraq. The porosity ranges from 15–20%, with permeability about 100 mD. In the Jambur oilfield, the Fatha Transition Zone is highly fractured and forms the main petroleum reservoir. The API gravity of the oils ranges from 12.9° to 41.0°, averaging 19.0° (Jassim and Goff, 2006). In the Mosul area, the limestone-dominated Transition Beds, at the base of the Fatha Formation, often contain heavy oil and bitumen. These are trapped by the overlying anhydrite-dominated unit.

Native sulphur is common in subsurface sections of the Fatha Formation, especially in the Mishraq area of northern Iraq. This region is regarded as one of the largest reserves of sulfur in the world (British Sulphur Corporation, 1974).

CONCLUSIONS

The Miocene (Langhian?) Fatha Formation (previously *Lower Fars Formation*) was deposited as a transgressive-regressive sequence in a broad shallow foreland basin adjacent to the Zagros-Taurides collisonal belt. Depositional settings ranged from open-marine and restricted-hypersaline to supratidal and continental (sabkha, fluvio-deltaic and exposure). It is bounded below by a regional sequence boundary (above the Jeribe Formation) that passes laterally to an unconformity that cuts into Eocene formations (i.e. Oligocene hiatus in part). The upper sequence boundary with the Injana Formation (previously Middle and Upper Fars Formation) is conformable.

A characteristic depositional feature of the Fatha Formation is high-frequency cycles of alternating mudrocks, limestones, gypsum and/or anhydrite and halite. Samples from these lithofacies were studied using petrographic and geochemical analysis (scanning electron microscopy, X-ray diffraction, geochemistry of major and trace elements), resulting in an improved interpretation of their depositional settings.

We propose a basin-center evaporitic model for the depositional regime of the Fatha Formation. The model is manifested by a predominance of continental sediments (red and variegated marls, silt and fine sandstones) along the margins of the basin. These increase upward, indicating shallowing-upwards and reduced accommodation space. The basin-center model is also manifested by the concentric arrangement of evaporites beds interbedded with limestone and marly limestone: from

predominantly gypsum and anhydrite along the margins to soluble halite in the depocenter. During high-frequency sea-level lowstands, intra-basinal and regional structural barriers may have isolated the hypersaline basin from the open sea, such that evaporation exceeded the ingress of water in an arid climate.

ACKNOWLEDGEMENTS

The authors thank the Deutsche Akademische Austausch Dienst (DAAD) for funding a three-month research visit to Bonn University for the first author. Furthermore, we thank the Geological Institute at Bonn University for providing access to their facilities. In particular we thank Herr Schmidt (Geochemistry), Mr. Georg Oleschinski (SEM), Mineralogical Institute (thin section photography) and Mrs. Iris Gebhardt for her valuable help in producing the figures and diagrams. The authors thank GeoArabia's Editor-in-Chief and three anonymous reviewers for their useful suggestions and assistance in editing the manuscript. We also thank Nestor Niño Buhay for designing the final paper for publication.

REFERENCES

Adams, C.G. 1992. Larger foraminifera and the dating of Neogene events. In, R. Tsuchi and J.C. Ingle Jr. (Eds.), Pacific Neogene Environment. Evolution and Events, University of Tokyo Press, Japan, p. 221-235.

Ahmad, N.M. 1980. Facies of the fossiliferous limestone beds of the Lower Fars Formation at some localities in northern Iraq. Unpublished MSc Thesis, Mosul University, Iraq, 215 p.

Aissaoui, D.M. 1985. Botryoidal aragonite and its diagenesis. Sedimentology, v. 32, p. 345-361.

Al-Banna, N.Y. (2008). Oligocene/Miocene boundary in northern Iraq. GeoArabia, Vol.13, No. 2, 163-166.

Al-Delemi, O.Kh.M.S. 2006. Sedimentology of the Pila Spi Formation dolomite and the overlying conglomerate in Bandwaya, Bashiqa, Maqlub areas, north Iraq. Unpublished MSc Thesis, Mosul University, Iraq, 86 p.

Al-Hashimi, H.A.J. and R.M. Amer 1985. Tertiary Microfacies of Iraq. Directorate General for Geological Survey and Mineral Investigation, Baghdad, Iraq, 56 p.

Allen, P.A., P. Homewood and G.D. Williams 1986. Foreland basins: An introduction. In, P.A. Allen and P. Homewood (Eds.), Foreland Basins. International Association of Sedimentologists, Special Publication no. 8, p. 3-12.

Al-Juboury, A.I. 1994. Petrology and provenance of the Upper Fars Formation (Upper Miocene), Northern Iraq. Acta Geologica Universitatis Comenianae, Bratislava, v. 50, p. 45-53.

Al-Juboury, A.I, S.Q. Al-Naqib and A.M. Al-Juboury 2001. Sedimentology, mineralogy and depositional environments of the clastic units, Fat'ha Formation (Middle Miocene), south of Mosul, Iraq. Dirasat, Pure Sciences, Jordan, v. 28, p. 80-105.

Al-Juboury, A.I, S.Q. Al-Naqib and A.M. Al-Tarif 2006. Mineralogical and geochemical study of the subsurface acidification products ninivite, alunite and jarosite, northern Iraq. Journal of the Association of Arab Universities for Basic and Applied Sciences (JAAUBAS), Bahrain, v. 2, p. 57-71.

Al-Juboury, A.I., A.M. Al-Tarif and M.I. Al-Eisa 2007. Basin analysis of the Burdigalian and Early Langhian successions, Kirkuk Basin, Iraq. In, B.C. Schreiber, S. Lugli and M. Babel (Eds.), Evaporites through Space and Time. Geological Society of London, Special Publication no. 285, p. 53-68.

Al-Marsoumi, A. 1980. Geochemistry and petrography of the Lower Fars evaporites in selected sections, Northern Iraq. MSc Thesis, University of Baghdad, Iraq (in Arabic, unpublished), 170 p.

Al-Mubarak, M. and R. Youkhana 1977. The regional geological mapping of Al-Fatha-Mosul area. State Organization for Minerals Library Reports, Baghdad, Iraq, no. 753.

Al-Naqib, S.Q. and T.A. Aghwan 1993. Sedimentological study of the clastic units of the Lower Fars Formation. Iraqi Geological Journal, v. 26, p. 108-121.

Al-Rawi, Y.T., A.S. Sayyab, J.A. Al-Jassim, M. Tamar-Agha, A.I. Al-Sammarai, S.A. Karim, M.A. Basi, D. Hagopian, K.M. Hassan, M. Al-Mubarak, A. Al-Badri, S.H. Dhiab, F.M. Faris and F. Anwar 1993. New names for some of the Middle Miocene-Pliocene formations of Iraq (Fat'ha, Injana, Mukdadiya and Bai Hassan formations). Iraqi Geological Journal, v. 25, p. 1-17.

Al-Sawaf, F.D.S. 1977. Sulfate reduction and sulfur deposition in the Lower Fars Formation, Northern Iraq. Economic Geology, v. 72, p. 608-618.

Al-Sharhan, A.S. and A.E.M. Nairn 1997. Sedimentary Basins and Petroleum Geology of the Middle East, Elsevier, Amsterdam, 843 p.

Aqrawi, A.A.M. 1993. Miocene evaporitic sequence of the southern Mesopotamian Basin. Marine and Petroleum Geology, v. 10, no. 2, p. 172-179.

Aswad, K.J., M.A. Amin and S.Q. Al-Naqib 1995. Marl-H2S interaction under surficial oxidizing conditions. Dirasat (Pure and Applied Sciences), Jordan, v. 22, no. 6, p. 1541-1561.

Barker, J.M., D.E. Cochran and R. Semrad 1979. Economic geology of Mishraq native sulfur deposits, northern Iraq. Economic Geology, v. 74, p. 484-495.
Beydoun, Z.R. 1991. Arabian plate hydrocarbon geology and potential: A plate tectonic approach. American Association of Petroleum Geologists, Studies in Geology, v. 33, p. 1-77.
British Sulphur Corporation 1974. Iraq emerges as a major sulphur exporter. Sulphur, no. 111, p. 36-40.
Buday, T. 1973. The regional geology of Iraq. Unpublished report, State Organization for Minerals Library Reports, Baghdad, Iraq.
Buday, T. 1980. The Regional Geology of Iraq. Stratigraphy and Palaeontology. Geological Survey and Mineralogical Investigations, Baghdad, Iraq, 445 p.
Buday, T. and S.Z. Jassim 1987. The Regional Geology of Iraq, Tectonism, Magmatism and Metamorphism. Publication of the Geological Survey of Iraq, 352 p.
Busk, H.G. and H.T. Mayo 1918. Some notes on the geology of the Persian oilfields. Institute of Petroleum Technology, v. 5.
Chamley, H. 1989. Clay Sedimentology. Springer-Verlag, Berlin, 623 p.
Curran, A.H. 1985. Biogenic Structures: Their Use in Interpreting Depositional Environments. Society of Economic Paleontologists and Mineralogists, Special Publication no. 35, 347 p.
Daniel, E.J. 1954. Fractured reservoirs of the Middle East. American Association of Petroleum Geologists Bulletin, v. 38, p. 774-815.
Dunnington, H.V. 1958. Generation, accumulation and dissipation of oil in Northern Iraq. In, L.G. Weeks (Ed.), Habitat of Oil. American Association of Petroleum Geologists, p. 1194-1251.
Dunnington, H.V. 1968. Salt-tectonic features of northern Iraq. Geological Society of America, Special Paper no. 88, p. 183-227.
Ehrenberg, S.N., N.A.H. Pickard, G.V. Laursen, S. Monibi, Z.K. Mossadegh, T.A. Svånå, A.A.M. Aqrawi, J.M. McArthur and M.F. Thirlwall 2007. Strontium isotope stratigraphy of the Asmari Formation (Oligocene-Lower Miocene), SW Iran. Journal of Petroleum Geology, v. 30, no. 2, p. 107-128.
Gill, W.D. and M.A. Ala 1972. Sedimentology of Gachsaran Formation (Lower Fars Series), Southwest Iran. American Association of Petroleum Geologists Bulletin, v. 56, no. 10, p. 1965-1974.
Goff, J.C., R.W. Jones and A.D. Horbury 1995. Cenozoic basin evolution of the northern part of the Arabian Plate and its control on hydrocarbon habitat. In, M.I. Al-Husseini (Ed.), Middle East Petroleum Geosciences Conference, GEO'94. Gulf PetroLink, Bahrain, v. 1, p. 402-412.
Fort, R. and M. Bustillo 1986. Estudio geologico de los yesos miocenos de la zona este de la cuenca de Madrid. Estudios Geologicos, v. 42, p. 387-395.
Hagopian, D. and C. Vejlupek 1977. Report on regional geological mapping of Mosul-Arbil area. State Organization for Minerals Library Reports, Baghdad, Iraq, no. 741.
Haq, B.U., J. Hardenbol and P.P. Vail 1987. The chronology of fluctuating sea level since the Triassic. Science, v. 235, p. 1156-1167.
Hasan, K.F. 1985. Study of foraminifera of the Lower Fars Formation in Al-Fatha area. Unpublished MSc Thesis, Baghdad University, Iraq, 91 p.
James, C.A. and J.G. Wynd 1965. Stratigraphic nomenclature of Iranian oil consortium agreement area. American Association of Petroleum Geologists Bulletin, v. 49, p. 835-870.
Jassim, S.Z. and S.A. Karim 1984. Final report on the regional geological survey of Iraq. Vol. 4, Paleogeography. State Organization for Minerals Library Reports, Baghdad, Iraq, 65 p.
Jassim, S.Z. and S.Q. Al-Naqib 1989. Ninivite: A new form of porcelainite and the associated alunite and jarosite minerals. A suite related to sulphuric acid seepage south of Mosul, Northern Iraq. Journal of the Geological Society of Iraq, v. 22, no. 1, p. 112-122.
Jassim, S.Z. and T. Buday 2006. Latest Eocene-Recent Megasequence AP11. In, S.Z. Jassim and J.C. Goff (Eds.), Geology of Iraq. Chapter 14, p. 169-184. Dolin and Moravian Museum, Czech Republic.
Jassim, S.Z. and J.C. Goff 2006. Geology of Iraq. Dolin, Prague and Moravian Museum, Czech Republic, 395 p.
Jassim, S.Z., S.A. Karim, M. Basi, M.A. Al-Mubarak and J. Munir 1984. Final report on the regional geological survey of Iraq. Vol. 3, Stratigraphy. Geological Survey of Iraq, Baghdad, Iraq.
Jassim, S.Z., A.S. Jibril and N.M.S. Numan 1997. Gypsum karstification in the Middle Miocene Fatha Formation, Mosul area, northern Iraq. Geomorphology, v. 18, p. 137-149.
Jassim, S.Z., R. Raiswell and S.H. Bottrell 1999. Genesis of the Middle Miocene stratabound sulphur deposits of northern Iraq. Journal of the Geological Society of London, v. 156, p. 25-39.
Jones, R.W. and A. Racey 1994. Cenozoic stratigraphy of the Arabian Peninsula and Gulf, In, M.D. Simmons (Ed.), Micropaleontology and Hydrocarbon Exploration in the Middle East. Chapman and Hall, New York, p. 273-307.
Jordan, T.E. 1981. Thrust loads and foreland basin evolution, Cretaceous, western United States. Bulletin of the American Association of Petroleum Geologists, v. 65, p. 2506-2520.
Khalaf, S.K. 1988. Middle Miocene ostracoda from Northern Iraq. In, T. Hanai, N. Ikeya and K. Ishizaki (Eds.), Evolutionary Biology of Ostracoda, its Fundamentals and Applications. Proceedings of the Ninth International Symposium on Ostracoda, Japan, p. 1113-1125.

Khalaf, S.K. 1994. On some Middle Miocene ostracoda from north Iraq and their paleoecological indications. Iraqi Geological Journal, v. 27, no. 3, p. 200-228.
Kinbell, T.N. and J.D. Humphrey 1994. Geochemistry and crystal morphology of aragonite cement of mixing zone origin, Barbados, West Indies. Journal of Sedimentary Research, v. A64, no. 3, p. 604-614.
Krauskopf, K.B. 1979. Introduction to Geochemistry, Second Edition. McGraw Hill, New York, 617 p.
Lawa, F.A. 1995. Marine and non-marine ichnofossils of the Middle and Upper Miocene sediments in the area between Mosul and Qaiyarah, North of Iraq. Iraqi Geological Journal, v. 28, p. 185-194.
Ma'ala, K.A., S.F. Mahdi, S.Q. Al-Naqib and F.A. Lawa 1988. Detailed geological mapping of Mosul-Fatha area for sulphur exploration. General Directorate of Geological Survey and Minerals Investigation, 483 p.
Metwalli, M.H., G. Philip and M.M. Moussly 1974. Petroleum-bearing formations in northeastern Syria and Northern Iraq. American Association of Petroleum Geologists Bulletin, no. 58, p. 1781-1796.
Mohi Al-Din, R.M., V.K. Sissakian, N.S. Yousif, R.M. Amin and S.H. Rofa 1977. The regional geological mapping of Mosul-Tel Afar area. State Organization for Minerals Library Reports, Baghdad, Iraq, no. 758.
Mustafa, A.A.M. 1980. Sedimentological studies of the Lower Fars Formation in the Sinjar Basin, Iraq. Unpublished MSc Thesis, Mosul University, Iraq, 243 p.
Numan, N.M.S. 1984. Basement controls of stratigraphic sequences and structural patterns in Iraq. Journal of the Geological Society of Iraq, v. 16, p. 8-24.
Numan, N.M.S.1997. A plate tectonic scenario for the Phanerozoic succession in Iraq. Journal of the Geological Society of Iraq, v. 30, p. 85-110.
Nunn, J.A. and N.B. Harris 2007. Subsurface seepage of sea water across a barrier: A source of water and salt to peripheral salt basins. Geological Society of America Bulletin, v. 119, nos. 9-10, p. 1201-1217.
Peryt, T.M. 2001. Gypsum facies transitions in basin-marginal evaporites: Middle Miocene (Badenian) of west Ukraine. Sedimentology, v. 48, p. 1103-1119.
Playa, E., F. Orti and F.L. Rosell 2000. Marine to non-marine sedimentation in the Upper Miocene evaporites of the Eastern Betics, SE Spain: Sedimentological and geochemical evidence. Sedimentary Geology, v. 133, p. 135-166.
Ponikarov, V.P., V.G. Kazmm, I.A. Mikhailov, A.V. Razvaliayev, V.A. Krasheninnikov, V.V. Kozlev, E.D. Soulid-Kondratiyer, K.Ya. Mikhailov, V.V. Kulakov, V.A. FaradzHev and K.M. Mirzayev 1967. The Geology of Syria, pan I, stratigraphy, igneous rocks and tectonics. Department of Geology and Mineralogy. Ministry of Industry, Syria, 230 p.
Prazak, J. 1978. The development of the Mesopotamian Basin during the Miocene. Journal of the Geological Society of Iraq, v. 11, p. 170-189.
Rouchy, J.M, C. Taberner, M.-M. Blanc-Valleron, R. Sprovieri, M. Russell, C. Pierre, E. Di Stefano, J.J. Pueyo, A. Caruso, J. Dinares-Turell, E. Gomis-Coll, G.A. Wolff, G. Cespuglio, P. Ditchfield, S. Pestrea, N. Combourieu-Nebout, C. Santisteban and J.O. Grimalt 1998. Sedimentary and diagenetic markers of the restriction in a marine basin: The Lorca Basin (SE Spain) during the Messinian. Sedimentary Geology, v. 121, p. 23-55.
Roveri, M., V. Manzi, F.R. Lucci and S. Rogledi 2003. Sedimentary and tectonic evolution of the Vena del Gesso Basin (Northern Appennine, Italy): Implications for the onset of the Messinian salinity crisis. Geological Society of America Bulletin, v. 115, no. 4, p. 387-405.
Salvany, J.M., A. Munos and A. Perez 1994. Nonmarine evaporitic sedimentation and associated diagenetic processes of the southwester margin of the Ebro Basin (Lower Miocene) Spain. Journal of Sedimentary Research, v. A64, no. 2, p. 190-203.
Searle, M.P. 2007. Strucural geometry, style and timing of deformation in the Hawasina Window, Al Jabal al Akhdar and Saih Hatat culminations, Oman Mountains. GeoArabia, v. 12, no. 2, p. 99-130.
Seilacher, R.A. 1967. Bathymetry of trace fossils. Marine Geology, v. 5, p. 413-426.
Sharland, P.R., R. Archer, D.M. Casey, R.B. Davies, S.H. Hall, A.P. Heward, A.D. Horbury and M.D. Simmons 2001. Arabian Plate Sequence Stratigraphy. GeoArabia Special Publication 2, Gulf PetroLink, Bahrain, 371 p.
Sharland, P.R., D.M. Casey, R.B. Davies, M.D. Simmons and O.E. Sutcliffe 2004. Arabian Plate Sequence Stratigraphy - Revision to SP2. GeoArabia, v. 9, no. 1, p. 199-219.
Shawkat, M.G. and M.E. Tucker 1978. Stromatolites and sabkha cycles from the Lower Fars Formation (Miocene) of Iraq. Geologische Rundschau, v. 67, p. 1-14.
Simmons, M.D., P.R. Sharland, D.M. Casey, R.B. Davies and O.E. Sutcliffe 2007. Arabian Plate Sequence Stratigraphy: Potential implications for global chronostratigraphy. GeoArabia, v. 12, no. 4, p. 101-130.
Stöcklin, J. 1968. Salt deposits of the Middle East. Geological Society of America, Special Paper no. 88, p. 158-181.
Sugden, W. 1951. Report on the stratigraphy and structure of the Lower Fars of Kirkuk oilfield. Iraq National Oil Company, Unpublished Report, 40 p.
Sulayman, M.D. 1990. Geochemistry, petrology, origin and diagenesis of gypsum rocks of Lower Fars Formation at Butma West area, northern Iraq. Unpublished MSc Thesis, Mosul University, Iraq, 175 p.
Sun, S.Q. 1995. Dolomite reservoirs: Porosity evolution and reservoir characteristics. American Association of Petroleum Geologists Bulletin, v. 79, no. 2, p. 186-204.
Taufiq, J.M. and J. Domas 1977. The regional geological mapping of Dohuk-Ain Zala area. State Organization for Minerals Library Reports, Baghdad, Iraq, no. 837.

Tucker, M.E. 1993. Carbonate diagenesis and sequence stratigraphy. In, V.P. Wright (Ed.), Sedimentology Review. Blackwell Scientific Publications, v. 1, p. 51-72.
Tucker, M. 1999. Sabkha cycles, stacking patterns and controls: Gachsaran (Lower Fars/Fatha) Formation, Miocene, Mesopotamian Basin, Iraq. Neues Jarhbuch Für Geologie Und Paläontologie, v. 214, p. 45-69.
van Bellen, R.C., H.V. Dunnington, R. Wetzel and D. Morton 1959. Lexique Stratigraphique International. Asie, Fase, 10a, Iraq, Paris, 333 p.
Warren, J.K. 2006. Evaporites: Sediments, Resources and Hydrocarbons. Springer, 1035 p.
Wright, L.D. and J.M. Coleman 1974. Mississippi River mouth processes: Effluent dynamics and morphologic development. Journal of Geology, v. 82, p. 751-778.
Yakta, S. 1976. Sedimentology of Fars group in Hadar area. State Organization for Minerals Library Reports, Baghdad, Iraq, no. 739.

ABOUT THE AUTHORS

Ali Ismail Al-Juboury *is a Professor and Researcher in the Petrology and Mineralogy of Sedimentary Rocks at the Research Center for Dams and Water Resources of Mosul University, Iraq. He also teaches at the Geology Department of Mosul University and supervises postgraduate students. Ali received his BSc in Geology and MSc in Sedimentology from Mosul University in 1980 and 1983, respectively, and his PhD from Cormenius University, Slovakia in 1992. Ali is a member of numerous international societies and has published several papers on sedimentology, mineralogy and geochemistry in Iraqi and international journals.*

alialjuboury@yahoo.com

Tom McCann *is a Professor of Sedimentology at Bonn University in Germany. He received his BA(Mod) from Trinity College Dublin, followed by his MsC from the University of New Brunswick in Canada, his PhD from Leicester University, England and his Habilitation from Potsdam University, Germany. Tom research concentrates on clastic sedimentology, particularly on the relationship between tectonics and sedimentation. Currently, he is doing outcrop-oriented studies in Bulgaria and Northern Spain.*

tmccann@uni-bonn.de

Manuscript Received June 3, 2007

Revised December 10, 2007

Accepted January 27, 2008

Press version proofread by the authors March 6, 2008